AGU100 ADVANCING EARTH AND SPACE SCIENCE

Tectonics

RESEARCH ARTICLE
10.1029/2017TC004899

Key Points:
- Paleomagnetism of Mesozoic red beds and Pliocene-Holocene basalts from Yunnan, China; blocks rotations along the Gaoligong shear zone
- Red beds yield CW rotations that reach 176 degrees close to fault and decrease moving away from it, up to be annulled at ~20 km distance
- Pliocene-Holocene basalts do not rotate; rotations likely occurred during the Oligo-Miocene activity of the Gaoligong shear zone

Supporting Information:
- Supporting Information S1
- Figure S1
- Data Set S1

Correspondence to:
F. Speranza,
fabio.speranza@ingv.it

Citation:
Pellegrino, A. G., Zhang, B., Speranza, F., Maniscalco, R., Yin, C., Hernandez-Moreno, C., & Winkler, A. (2018). Tectonics and paleomagnetic rotation pattern of Yunnan (24°N–25°N, China): Gaoligong fault shear versus megablock drift. *Tectonics*, *37*. https://doi.org/10.1029/2017TC004899

Received 20 NOV 2017
Accepted 11 APR 2018
Accepted article online 20 APR 2018

©2018. American Geophysical Union. All Rights Reserved.

Tectonics and Paleomagnetic Rotation Pattern of Yunnan (24°N–25°N, China): Gaoligong Fault Shear Versus Megablock Drift

Alessandra G. Pellegrino[1], Bo Zhang[2], Fabio Speranza[3], Rosanna Maniscalco[1], Congyuan Yin[2], Catalina Hernandez-Moreno[3], and Aldo Winkler[3]

[1]Università degli Studi di Catania, Dipartimento di Scienze Biologiche, Geologiche e Ambientali, Catania, Italy, [2]School of Earth and Space Science, Peking University, Beijing, China, [3]Istituto Nazionale di Geofisica e Vulcanologia, Rome, Italy

Abstract A wealth of paleomagnetic data from Yunnan (China) showed in the past a predominant post-Cretaceous clockwise (CW) rotation pattern, mostly explained invoking huge (hundreds of kilometer wide) blocks, laterally escaping (and/or rotating) due to India-Asia collision, separated by major strike-slip shear zones. Here we report on the paleomagnetism of the outcrops close to the Gaoligong dextral shear zone. Fifty paleomagnetic sites (503 samples) were sampled at variable distances (up to ~25 km) from mylonites exposed along the fault. Eighteen Jurassic-Cretaceous red bed sites yield systematic CW rotations with respect to Eurasia that peak at maximum (176°) close to the fault, and progressively decrease moving eastward, up to be virtually annulled ~20 km east of mylonite contact. West of the fault, 15 Pliocene-Holocene sites from the Tengchong volcanic field do not rotate. Thus, our data show that Gaoligong shear zone activity yielded significant CW rotations that were likely coeval to the main Oligo-Miocene episodes of dextral fault shear. The Gaoligong zone rotation pattern conforms to a quasi-continuous crust kinematic model and shows blocks of ≤1 km size close to the fault that enlarge moving eastward. Rotation values and width of the rotated-deformed zone translate to a 230–290 km Gaoligong shear zone dextral offset. Our work shows that fault shear plays a significant role for Indochina CW rotation occurrence. However, significant rotations at distances >30 km from main faults were also documented, so that additional tectonics—whose relative relevance has not been elucidated yet—must contribute as well to the rotation pattern.

1. Introduction

To the SE of Tibet, the Indochina block is thought to have been extruded southeastward during the initial phases of India-Eurasia collision (Molnar et al., 1988; Molnar & Tapponnier, 1975; Patriat & Achache, 1984; Replumaz & Tapponnier, 2003). Northern Indochina is bounded by two major shear zones, the Ailao Shan-Red River shear zone to the east, and Sagaing fault system to the west (Figure 1). Within the block itself, two additional ~N-S shear zones occur: the Gaoligong and Biluoxueshan-Chongshan shear zones. Significant paleomagnetic rotations have been documented in Yunnan, straddling the northern Indochina block and the southeastern Tibetan Plateau (Figure 1 and Table 1). Paleomagnetic data were mostly gathered from Cretaceous continental red beds and showed a predominant clockwise (CW) rotation pattern extending for about 1,000 km in the 22°–25°N latitude range (Li, Advokaat, et al., 2017; Tong et al., 2016, and references therein).

Although the paleomagnetic data set from Yunnan is undoubtedly robust, the tectonic explanations for such rotational pattern remain still not completely convincing. A first set of models suggests that CW rotations of Yunnan are the result of lateral escape of Tibet that rotated CW around the northeastern corner of the Indian Plate (e.g., Chen et al., 1995; Funahara et al., 1992, 1993; Kondo et al., 2012; Sato et al., 2001, 2007; Tanaka et al., 2008; Tong et al., 2013). However, this may explain CW rotations of the northern part of Indochina but can hardly account for the CW rotations documented further south, at 21°–22°N latitudes.

A second set of models (Gao et al., 2015; S. Li, Advokaat, et al., 2017; G. Wang et al., 2008; Zhao et al., 2015) argues that CW rotations occur along rigid megablocks (hundreds of kilometers wide) or slates bounded by strike-slip faults, conforming to the so-called "bookshelf" tectonics (Cowan et al., 1986; Garfunkel & Ron, 1985; Mandl, 1987; McKenzie & Jackson, 1986; Nur et al., 1986; Ron et al., 1984). This model is hard to maintain—at least for the northern Yunnan—as the elongated slates located between the faults are some

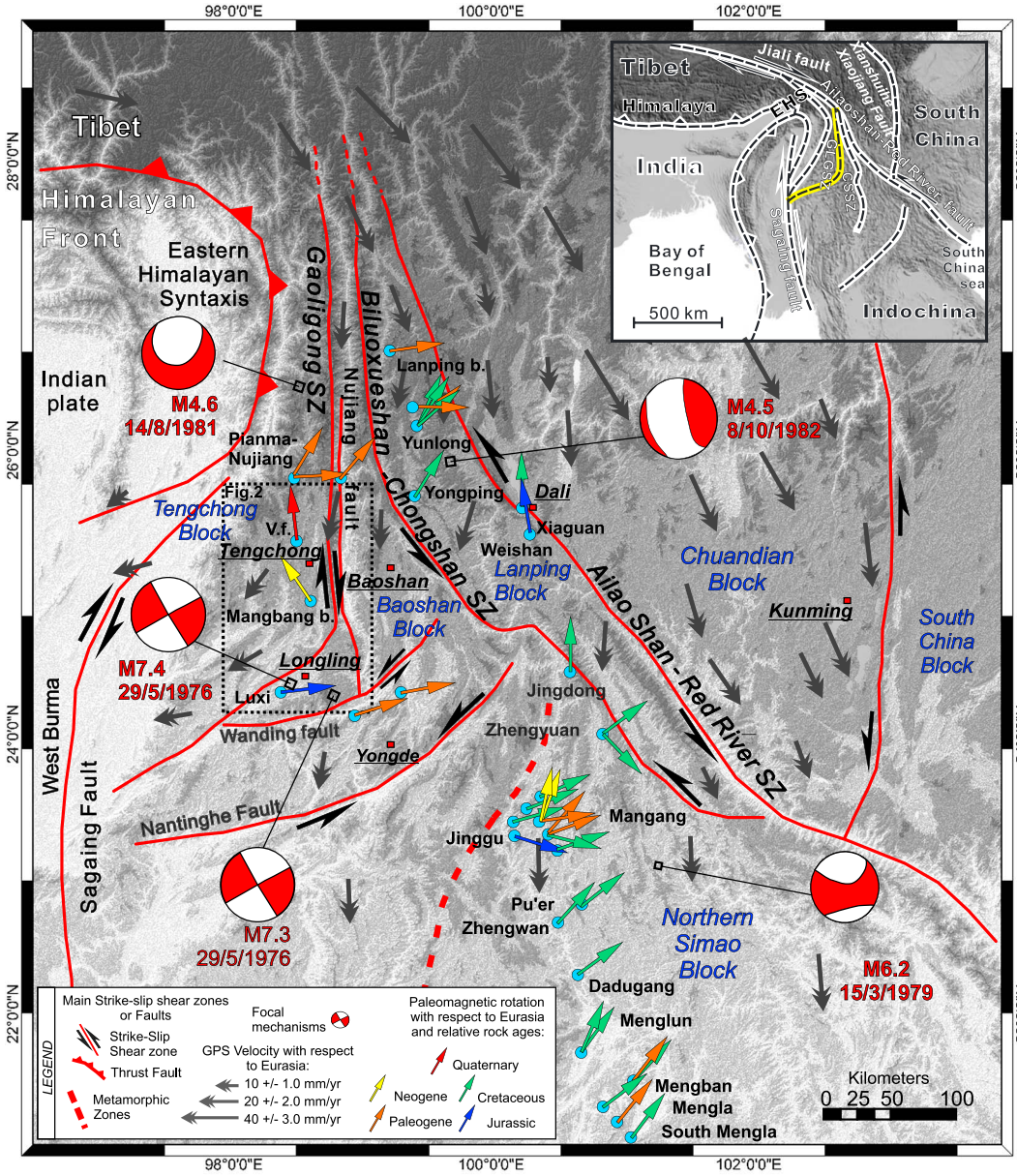

Figure 1. Map of western Yunnan and southeastern Eastern Himalayan Syntaxis, main tectonic features, and synthesis of the main seismological, geodetic, and paleomagnetic data. Base map source: Esri, UserCommunity, geographic information system, Coordinate System & Projection: world geodetic system 1984-Web Mercator Auxiliary Sphere. Focal mechanisms are derived from the Harvard Global Centroid Moment Tensor Catalog (Dziewonski et al., 1981; Ekström et al., 2012). Yellow thin arrows show present-day global positioning system velocities around the Tibetan Plateau relative to stable Eurasia (Liang et al., 2013). Colored arrows (see legend) represent paleomagnetic rotations with respect to Eurasia, recalculated from previous paleomagnetic results (see table 1), according to Demarest (1983) and using updated Eurasia (from 170 to 140 Ma) and East Asia (from 130 to 10 Ma) poles by Torsvik et al. (2012) and Cogné et al. (2013), respectively.

1,000 km long and only 200–300 km wide (Figure 1), so that their rotations would lay a significant space problem. Alternatively, the land stripes between the faults might be broken into several small slates, each rotating independently, of which, however, no field evidence has been found so far.

There is a third tectonic mechanism possibly yielding vertical-axis rotations that has not been investigated in Indochina so far: strike-slip fault shear. In fact, it has been observed that strike-slip zones are bounded by damage zones where large (even >90°) vertical-axis rotations may occur in response to the ductile

Tectonics

10.1029/2017TC004899

Table 1

Paleomagnetic Site-Mean Directions Obtained From Previous Studies in Triassic-Neogene Rocks From Yunnan, and Updated Rotation and Flattening Values With Respect to Eurasia Calculated Using Paleopoles by Torsvik et al. (2012) and Cogné et al. (2013)

Locality	Geographic coordinates		Series/ epoch	Numerical age (Ma)	N	Considered paleopoles age	Observed direction					Recalculated by us		Reference
							In Situ		Tilt corrected			Rotation	Flattening	
	Latitude (°N)	Longitude (°E)					D (deg)	I (deg)	D (deg)	I (deg)	α_{95} (deg)	$R \pm \Delta R$	$F \pm \Delta F$	
Tengchong Block														
Pianma-Nujiang	26.0	98.7	Oligocene	30	6	30	38.5	20.0	33.3	41.4	24.5	31.2 ± 26.3	−5.0 ± 19.4	Kornfeld, Eckert, Appel, Ratschbacher, Sonntag, et al. (2014)
	26.0	98.7	Eocene	40	6	40	84.5	14.9	89.8	35.1	11.8	87.2 ± 11.8	−1.6 ± 10.5	Kornfeld, Eckert, Appel, Ratschbacher, Sonntag, et al., (2014)
Tengchong v.f	25.1	98.4	Pleistocene-Holocene	2.5–0	16	0	352.5	25.4	_	_	44.9	−7.5 ± 40.3	−5.7 ± 14.1	Kornfeld, Sonntag, et al. (2014)
Mangbang b.	24.8	98.6	Upper Miocene-Pliocene	14–2.5	16	10	327.3	48.7	_	_	14.1	−33.7 ± 17.3	−9.1 ± 11.3	Kornfeld, Sonntag, et al. (2014)
Baoshan Block														
Luxi	24.3	98.4	Middle Jurassic	163–174	6	170[a]	110.0	−2.9	99.7	35.2	11.3	81.3 ± 11.8	24.9 ± 9.3	Huang and Opdyke (1993)
Baoshan	26.0	98.8	Oligocene	30	16	30	32.6	51.8	42.2	47.0	7.8	40.0 ± 9.2	−10.6 ± 6.9	Kornfeld, Eckert, Appel, Ratschbacher, Pfänder, et al. (2014)
Yongde	24.4	99.3	Eocene-Oligocene	56–23	22	20	81.7	35.1	_	_	3.8	79.4 ± 4.4	0.2 ± 4.7	Y. Tong et al. (2016)
	24.2	99.0	Paleocene	66-56	5	60	_	_	76.9	17.8	3.8	72.5 ± 9.1	14.0 ± 9.5	Tong et al. (2016)
Lanping Block														
Yunlong	25.8	99.4	Middle Cretaceous	100	20	100	50.9	29.8	40.2	49.9	3.9	32.0 ± 5.6	−9.0 ± 4.8	Sato et al. (1999)
			Lower Cretaceous	145–100.5	23	120	103.2	61.6	59.7	41.0	11.9	49.3 ± 12.6	1.8 ± 9.7	Yang et al. (2001)
			Upper Cretaceous	100.5–66	9	80	52.4	62.1	34.0	52.4	7.3	24.0 ± 9.8	−15.4 ± 6.9	Yang et al. (2001)
			Paleocene	66–56	11	60	49.2	7.6	50.2	31.1	13.2	45.7 ± 12.5	3.2 ± 11.4	Yang et al. (2001)
Lanping area	26.4	99.3	Eocene	38–29	9	30	274.0	−35.6	263.8	−42.1	14.1	81.6 ± 15.1	−5.1 ± 11.4	Sato et al. (2001)
Yunlong area	25.9	99.4	Eocene	38–29	5	30	271.8	−19.8	273.0	−31.8	11.1	90.8 ± 10.5	4.4 ± 9.2	Sato et al. (2001)
Weishan	25.4	100.2	Upper Jurassic	163–145	5	150	356.5	34.5	7.3	25.3	10.4	−9.5 ± 10.8	28.6 ± 9.6	Huang and Opdyke (1993)
Xiaguan	25.6	100.2	Middle Cretaceous	100	9	100	8.9	59.2	6.9	47.7	8.6	−1.3 ± 10.4	−6.9 ± 7.6	Huang and Opdyke (1993)
Yongping	25.5	99.5	Lower Cretaceous	145–100.5	12	120	48.9	50.8	42.0	51.1	15.7	31.7 ± 20.0	−8.6 ± 12.6	Funahara et al. (1993)
Northern Simao Block														
Jinggu	23.4	100.9	Middle Cretaceous	100	8	100	73.2	67.7	79.4	43.3	9.1	71.3 ± 10.2	−5.4 ± 8.1	Huang and Opdyke (1993)
Jinggu	23.6	100.5	Middle Jurassic	174.1–163.5	10	170	75.5	31.4	83.3	36.8	5.4	65.8 ± 7.1	23.3 ± 5.2	Huang and Opdyke (1993)
Mengla	21.6	101.4	Middle Cretaceous	100	10	100	288.7	19.3	60.8	37.8	7.6	52.7 ± 8.0	−2.4 ± 7.2	Huang and Opdyke (1993)
Jinggu (Jingxing Fm.)	23.4	100.4	Lower Cretaceous	145–100.5	3	120	78.4	58.0	84.4	39.6	17.8	74.2 ± 18.4	0.3 ± 14.2	Chen et al. (1995)
Jinggu (Mangang Fm.)	23.4	100.5	Lower Cretaceous	145–100.5	3	120	294.2	23.1	297.5	−33.3	7.1	107.3 ± 7.0	6.6 ± 6.4	Chen et al. (1995)
	23.5	100.8	Lower Cretaceous	145–100.5	4	120	309.3	−6.2	294.4	−38.1	12.1	104.2 ± 12.3	2.0 ± 9.9	Chen et al. (1995)
Jinggu (Mengyujing Fm.)	23.5	100.8	Paleocene	66–56	9	10[a]	42.8	26.1	23.9	51.6	7.9	41.7 ± 7.2	11.7 ± 6.8	Chen et al. (1995)
Jinggu (Mengla Group)	23.5	100.7	Eocene-Oligocene	56–23	7	40	106.4	49.1	84.7	38.9	7.6	81.8 ± 8.3	−9.3 ± 8.0	Chen et al. (1995)
Jinggu (Sanhaogou Fm.)	23.5	100.7	Miocene	23–5.3	6	10	34.6	20.2	21.1	35.5	7.5	20.0 ± 7.5	2.3 ± 6.5	Chen et al. (1995)
Jinggu	23.5	100.8	Eocene	56–33.9	6	40	_	_	73.1	39.9	11.8	70.2 ± 12.5	−10.3 ± 10.6	Yang and Otofuji (2001)
Jingdong	24.5	100.8	Cretaceous	145–66	15	100	20.7	55.9	8.3	48.8	7.7	0.1 ± 9.6	−9.4 ± 7.1	Tanaka et al. (2008)
Zhengyuan	24.0	101.0	Cretaceous	145–66	14	100	94.7	88.2	61.8	46.1	8.1	53.6 ± 9.6	−7.4 ± 7.4	Tanaka et al. (2008)
West Zhengyuan	24.0	101.0	Cretaceous	145–66	5	100	315.6	−8.2	324.2	−49.4	6.4	136.0 ± 8.2	−10.7 ± 6.3	Tanaka et al. (2008)
South Mengla	21.4	101.6	Cretaceous	145–66	19	100	353.6	50.3	51.2	46.4	5.6	43.2 ± 7.0	−11.3 ± 6.0	Tanaka et al. (2008)
Pu'er	23.0	101.0	Cretaceous	145–66	31	100	82.4	49.5	59.9	45.2	5.1	51.8 ± 6.4	−7.9 ± 5.6	Sato et al. (2007)
Zhengwan	22.8	100.9	Upper Cretaceous	100–66	11	80	267.5	57.4	51.8	47.9	6.9	41.9 ± 8.5	−15.0 ± 6.8	Kondo et al. (2012)
Dadugang	22.4	101.0	Upper Cretaceous	100–66	12	80	78.1	69.0	64.1	48.1	7.3	54.2 ± 9.0	−15.8 ± 7.0	Kondo et al. (2012)
Mengban	21.8	101.6	Paleocene-Eocene	66–33.9	6	50	12.9	45.8	43.5	23.0	13.4	37.6 ± 12.3	6.1 ± 12.9	Tong et al. (2013)
Mengla	21.5	101.5	Eocene-Oligocene	56–23	17	40	32.3	34.0	41.8	23.8	5.8	38.8 ± 6.0	2.5 ± 7.2	Tong et al. (2013)
	21.4	101.6	Lower Cretaceous	145–100.5	14	120	10.7	40.1	46.9	42.2	7.7	36.8 ± 8.5	−4.8 ± 6.8	Tong et al. (2013)
Menglun	21.9	101.2	Upper Cretaceous	10–66	6	80	44.7	58.3	33.2	30.9	8.2	23.3 ± 8.0	0.6 ± 7.7	Tong et al. (2013)
	21.9	101.2	Lower Cretaceous	145–100.5	19	120	66.7	72.6	46.2	45.9	11.0	36.1 ± 12.6	−7.9 ± 9.2	Tong et al. (2013)

Table 1 *(continued)*

Locality	Geographic coordinates		Series/ epoch	Numerical age (Ma)	N	Considered paleopoles	Observed direction				Recalculated by us			Reference
							In Situ		Tilt corrected		Rotation	Flattening		
	Latitude (°N)	Longitude (°E)				age	D (deg)	I (deg)	D (deg)	I (deg)	α_{95} (deg)	$R \pm \Delta R$	$F \pm \Delta F$	
Mengban	21.8	101.6	Cretaceous	145–66	4	100	27.5	31.4	50.5	31.0	6.4	42.4 ± 6.5	4.7 ± 6.4	Tong et al. (2013)
Jinggu	23.5	100.4	Middle Cretaceous	100	47	100	73.4	42.8	77.0	43.0	2.9	68.9 ± 4.3	−5.1 ± 4.5	Gao et al. (2015)
	23.5	100.7	Miocene	23–5.3	38	10	32.3	26.9	13.7	36.0	3.3	12.6 ± 3.8	1.8 ± 3.9	Gao et al. (2015)
Jinggu	23.5	100.7	Miocene	23–5.3	10	10	16.4	15.4	13.5	32.2	5.8	12.4 ± 5.8	5.6 ± 5.4	S. Li, Yang, et al. (2017)
			Paleocene	66–56	12	20[a]	43.0	41.7	36.1	31.5	8.4	40.6 ± 9.2	−7.6 ± 7.5	S. Li, Yang, et al. (2017)
			Eocene	56–33.9	12	20[a]	27.8	32.1	35.2	35.7	6.5	25.4 ± 6.5	1.9 ± 6.3	S. Li, Yang, et al. (2017)
			Eocene	56–33.9	18	20[a]	37.0	32.8	53.0	33.6	4.3	34.6 ± 4.7	1.2 ± 5.0	S. Li, Yang, et al. (2017)
			Eocene-Oligocene	56–23	11	20[a]	34.9	33.2	38.4	37.3	9.7	32.5 ± 9.4	0.8 ± 8.4	S. Li, Yang, et al. (2017)
			Eocene-Oligocene	56–23	17	20[a]	35.2	20.2	38.6	33.0	5.7	32.8 ± 5.4	13.8 ± 5.8	S. Li, Yang, et al. (2017)
			Eocene-Oligocene	56–23	14	20[a]	45.0	22.8	50.8	31.8	5.8	42.6 ± 5.5	11.2 ± 5.8	S. Li, Yang, et al. (2017)

Note. Age in Ma is from the geologic timescale of Cohen et al. (2013). D and I are site-mean declination and inclination calculated before and after tectonic correction; α_{95} is statistical parameter after Fisher (1953); N is number of sites; site-mean rotation R and flattening F values, and relative errors ΔR and ΔF (according to Demarest, 1983) are relative to coeval D and I values expected at the sampling area from East Asia paleopoles by Cogné et al. (2013), excepet 150 and 170 Ma from East Asia poles by Torsvik et al. (2012).
[a]Post-tilting remagnetized sites, R and F values are calculated using the in situ D and I values.

deformation taking place in the lower crust (Beck, 1976; Hernandez-Moreno et al., 2014, and references therein; Kimura et al., 2011; Piper et al., 1997; Randall et al., 2011; Ron et al., 1984; Sonder et al., 1994). Depending upon fault displacement and locking, and crust rheology, such local rotation zone may be even 20–30 km wide on each fault side (Randall et al., 2011; Sonder et al., 1994).

In this paper, we investigate if—and to what extent—strike-slip fault shear may be responsible for the CW rotations widely documented in Yunnan. We selected the Gaoligong dextral shear zone and sampled 50 paleomagnetic sites at variable distances (up to ~25 km) from the contact with mylonites and metamorphic rocks exposed along the shear zone. Our work yields additional evidence to try unraveling the Indochina rotation pattern puzzle.

2. Eastward Drift of Tibet and Tectonic Deformation of East Asia

Since early Cenozoic times, the northward drift of Indian plate and its progressive indentation into Asia (Tapponnier & Molnar, 1977) are producing spreading and crustal deformation in SE Asia (Leloup et al., 2001; Morley, 2007; Roger et al., 1995; Searle, 2006; Tapponnier et al., 1986; Yin, 2010; Zhong & Tapponnier, 1990).

Plate collision yielded the 2,000-km wide and 5,000-m high Tibet Plateau, the most outstanding high-elevation plateau of the Earth (Besse et al., 1984; Najman et al., 2010; Searle et al., 2007). Since the Oligocene, plate convergence has been partly accommodated by the southeastward lateral extrusion along continental-scale strike-slip shear zones in the South China and Indochina blocks. Identifying and determining the role and kinematic variability of the continental-scale strike-slip faults, responsible for accommodating a significant portion of the post-50 Ma India-Eurasia convergence, have great significance to understand the geologic evolution during Tibet Plateau growth (Hall, 2002; Hall et al., 2008; Houseman & England, 1986, 1993; Molnar & Dayem, 2010; Peltzer & Tapponnier, 1988; Royden et al., 2008; Tapponnier et al., 1982, 1990; Vilotte et al., 1986; Wang & Burchfiel, 2000; Yin & Taylor, 2011).

The upper brittle crust of SE Tibet is characterized by a set of curved strike-slip faults, running around the northeastern edge of the Indian indenter (Eastern Himalayan Syntaxis, Figure 1), which are inferred to concentrate the deformation between major crustal blocks. In the past, the ductile high-temperature deformation of the shear zones, addressed by structural geology studies coupled with radiometric dating, traced an activity spanning a wide time window between 35 and 15 Ma (late Eocene to mid-Miocene; Leloup & Kienast., 1993; Leloup et al., 1995; Searle 2006; Searle et al., 2007, and references therein). However, the apparent lack of post-15 Ma shear zone activity conflicts with both GPS evidence (Figure 1; Liang et al., 2013), showing southward drift of Indochina at a ~2 cm/year rate, and significant seismic activity with mainly strike-slip focal mechanisms (Socquet & Pubellier, 2005).

There are two end-member models commonly used to interpret the deformation mechanisms of eastern and SE Tibet. The first is the "tectonic escape" model: strain is localized on a limited number of major faults bounding rigid lithospheric megablocks and is driven solely by stresses exerted at plate boundaries (Avouac & Tapponnier, 1993; Ji et al., 2000; Molnar & Tapponnier, 1975; Replumaz & Tapponnier, 2003; Tapponnier et al., 1982; Tapponnier & Molnar, 1976, 1977); the second is the "crustal flow" model: deformation is pervasive and driven, for a significant part, by buoyancy forces resulting from lateral variations of crustal thickness. Deformation of the crust is continuous, and there are no blocks separated by strike-slip faults (Bird, 1991; Clark & Royden, 2000; England & Houseman, 1986; Houseman & England, 1993; Royden et al., 1997). Additionally, E. Q. Wang and Burchfiel (1997) were the first to notice that the extrusion was accompanied by strong internal deformation and rotation of smaller crustal fragments. Clark et al. (2006) and Liu-Zeng et al. (2008) noticed

that Mesozoic-Cenozoic redbeds in northern Indochina are tightly folded around NNW trending fold axes, and Hall (2002) also suggested a major shortening in N-NW Indochina block. Finally, S. Li, Advokaat, et al. (2017) proposed that this shortening is in part accommodated by large-scale block rotations.

3. Tectonics of Yunnan and Characteristics of Its Major Shear Zones

The SE region of the Eastern Himalayan Syntaxis comprises three major tectonometamorphic megaterranes, called Tengchong, Baoshan, and Lanping-Simao blocks (Figure 1). They are characterized by different lithologies, protolith ages, intracontinental deformation, paleogeography, and orogenic history (Bureau of Geology and Mineral Resources of Yunnan Province, 1990; Bureau of Geology and Mineral Resources of Xizang Autonomous Region, 1993; Metcalfe, 2006; E. Q. Wang & Burchfiel, 1997; Zhong, 1998, 2000). Such megablocks are bounded by three ductile shear zones: the Ailao Shan-Red River, the Biluoxueshan-Chongshan (hereinafter referred as to Chongshan) and the Gaoligong shear zone (Akciz et al., 2008; Leloup et al., 1995; Lin et al., 2009).

The Ailao Shan-Red River shear zone is the major geological discontinuity that separates the Chuandian and South China blocks to the northeast from the Indochina block (Leloup et al., 1995; Tapponnier et al., 1990; J. J. Zhang et al., 2006; Zhong & Tapponnier, 1990). The shear zone extends over a length of $>$1,000 km between the South China Sea to the south and the Tibet Plateau to the north and stands out as the most striking discontinuity in the morphology and geology of Yunnan (Figure 1). It is regarded as the eastern boundary of the southeastward extruded Indochina block, in agreement with the observed left-lateral ductile shear (Leloup et al., 1995; Tapponnier et al., 1982; L. Zhang & Zhong, 1996). However, the timing and the amount of displacement along the shear zone have been strongly debated over the last decades. A left-lateral movement occurring from latest Eocene to early Miocene (35–17 Ma) has been inferred, with widely varying total slip estimates of 100–1,400 km, specifically between 700 ± 200 km in the NW and ~250 km in the SE (Chung et al., 1997; Fyhn, Boldreel, & Nielsen, 2009; Gilley et al., 2003; T. M. Harrison et al., 1996; Leloup et al., 1995; S. Li, Advokaat, et al., 2017; Schärer, Zhang, & Tapponnier, 1994; Searle, 2006; Tapponnier et al., 1990; E. Q. Wang & Burchfiel, 1997; E. C. Wang, Burchfiel, Royden, Chen, et al., 1998; P.-L. Wang, Lo, et al., 1998). Conversely, a dextral motion has been observed since 8–5 Ma, with a total slip estimated between 9 and 54 km (Allen et al., 1984; Replumaz et al., 2001; Schoenbohm et al., 2006; E. C. Wang, Burchfiel, & Royden, 1998).

The Chongshan shear zone extends for hundreds of kilometers along the Biluoxueshan-Chongshan Mountains in western Yunnan with a width of ~10 km. The shear zone is divided by a N-S trending fault into two belts with contrasting metamorphic facies: an eastern low-grade schist belt and a western high-grade gneiss belt, considered to be a paired-metamorphic zone (G. Wang et al., 2008; B. Zhang et al., 2010; B. Zhang, Zhang, Zhong, et al., 2012; R. Zhang et al., 1993; B. Zhang et al., 2011). The shear zone formed during the Cenozoic and exhumation (from a depth of approximately 20 km) occurred from late Eocene to Miocene times (Akciz et al., 2008).

The Chongshan shear zone shows tectonic deformation starting as early as late Paleocene times (57 Ma), and a shear sense that is inconsistent along its southern and northern branches (B. Zhang, Zhang, Chang, et al., 2012; B. Zhang et al., 2010, 2011). Along the northern segment of the zone a dextral displacement exceeding 100 km during the 57–16 Ma age window was reported, while left-lateral shear has been documented further south (B. Zhang et al., 2010). Sediments predominantly older than strike-slip fault activity are widely exposed in the Lanping block and are made almost entirely of a 7.5-km thick succession of continental red beds of Jurassic-early Cenozoic age.

4. The Gaoligong Shear Zone and Adjacent Blocks

The Gaoligong shear zone extends eastward and southward from the Eastern Himalayan Syntaxis forming the boundary between the Tengchong and Baoshan blocks (Figure 1; P. Li et al., 2004; Mitchell, 1992, 1993; Y. Xu et al., 2012). It is exposed completely along the Gaoligong Mountains west of the Nujiang river valley (Figure 2; E. Q. Wang & Burchfiel, 1997; G. Wang et al., 2008; Zhong, 2000), where dextral ductile shear indicators are widely preserved.

Field observations along the Gaoligong Mountains showed that the 500-m to 6-km wide Gaoligong shear zone contains mylonitic granites, gneisses, quartz schists, and marble lens and is characterized by steep

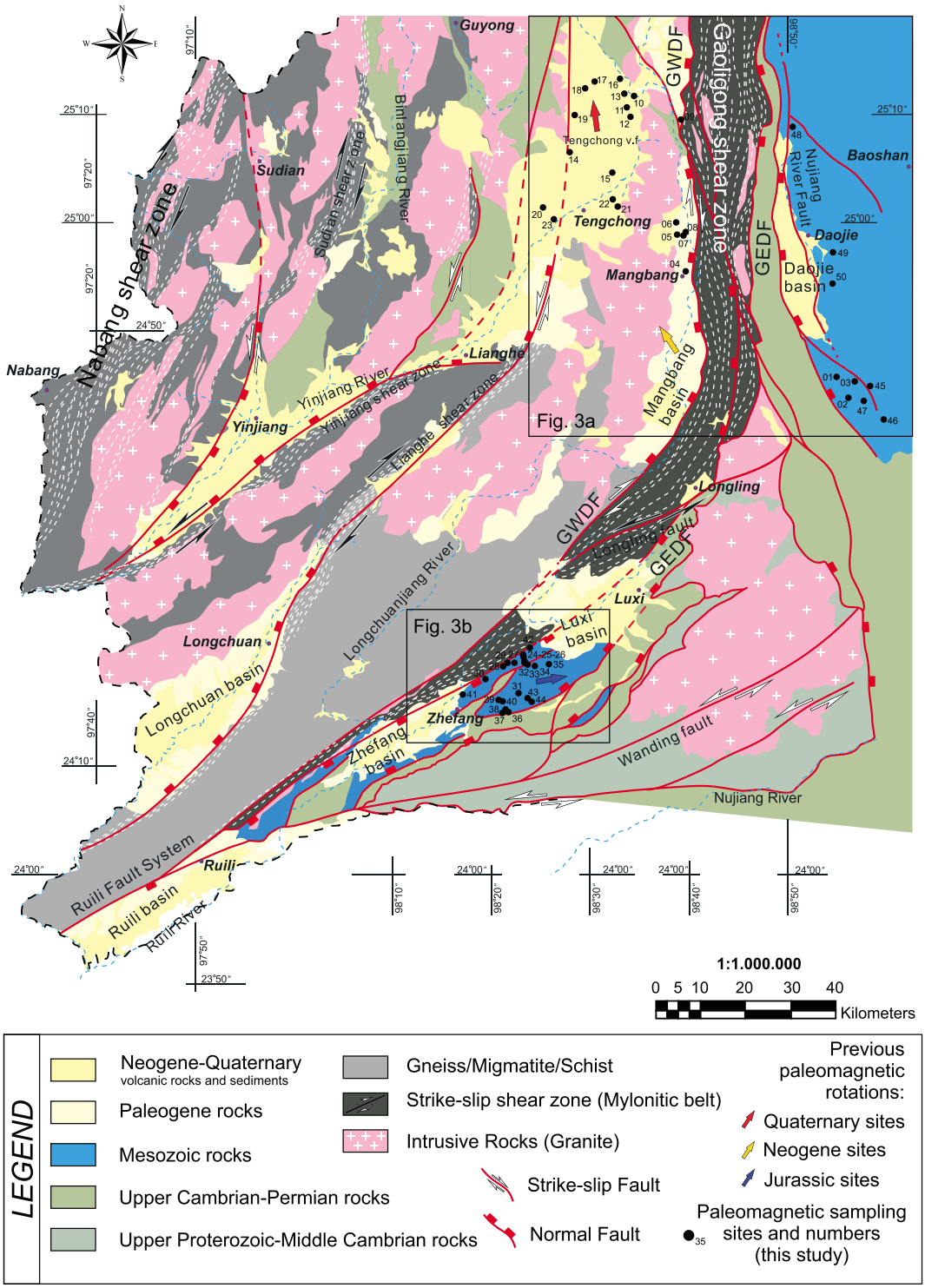

Figure 2. Simplified geological and tectonic map of the Gaoligong shear zone and adjacent areas. Boxes indicate the two areas of paleomagnetic investigation. GEDF = Gaoligong east detachment fault; GWDF = Gaoligong west detachment fault.

foliation and nearly N-S trending subhorizontal stretching lineations (G. Wang et al., 2008). The banded mylonitic rocks were tightly folded with the hinges parallel to the lineations (B. Zhang, Zhang, Chang, et al., 2012). The shear zone is truncated by brittle normal faults with dextral shear component along both sides of the mylonitic belt (Gaoligong detachment faults in Figure 2).

Moving southward, shear zone width increases from 10 to 20 km, and the mountains decrease in elevation from 3,500 m to 2,500 m. Near Longling, the mylonitic rocks of the Gaoligong shear zone curve to the southwest, are exposed at the southwest tip of the mountain range and finally crop out close to the Zhefang and Ruili basins (Figures 2 and 3b).

The age of activity and kinematics along the shear zone was constrained by several Ar/Ar ages and structural studies on ductile deformation that consistently suggest a dextral shear sense. Lin et al. (2009) and B. Zhang, Zhang, Zhong, et al. (2012) provided 13–18 and 10–16 Ma activity windows (respectively) relying on Ar/Ar mica ages, whereas an older 27–32 Ma activity age was radiometrically documented by Y. J. Wang et al. (2006). Ductile right-lateral deformation indicators are widespread all along the shear zone.

To the south, the Gaoligong shear zone is reactivated and truncated with left-lateral movement by the active NE trending Longling and Wanding brittle faults (G. Wang et al., 2008; Figures 1 and 2). Apatite fission track data by G. Wang et al. (2008) constrain the onset of left-lateral brittle fault activity between 8.4 and 0.9 Ma. More recent (and possibly ongoing) dextral strike-slip activity of the Gaoligong shear zone was proposed by Socquet and Pubellier (2005) relying on satellite image analysis. In agreement with the latter work, Morley (2007) suggested that the shear zone is a late Neogene transpressional deformation zone.

Seismic activity has been recorded along the southern NE trending part of the Gaoligong shear zone (also called Ruili fault system, Figure 2). On 29 May 1976, two large magnitude earthquakes ($Mw > 7$) occurred in the Longling area south of Tengchong (Y. J. Wang et al., 2006; S. C. Zhang et al., 1994). The first $Mw = 7.4$ event was located close to the NE trending Gaoligong shear zone branch (Holt et al., 1991). The second $Mw = 7.3$ event occurred close to the Wanding fault (Figure 1; Y. Xu et al., 2012). Both of them are strike-slip events with steep fault planes and ~N-S P axes and have been interpreted as related to left-lateral shear along NE trending Longling and Wanding faults (Figure 2; Y. J. Wang et al., 2006). It is noteworthy that the present-day sinistral kinematics along NE faults entering and cross cutting the southern branch of the Gaoligong shear zone is opposite to the dextral kinematics reported for Oligo-Miocene times.

The Tengchong block is bounded to the west by the dextral strike-slip Sagaing fault, whose activity started in early Miocene times with a total estimated displacement of 460 km (Curray, 2005; Mitchell, 1993). It is characterized at present by several right-lateral focal mechanisms, particularly along its northern end (Ratschbacher et al., 1996; Wang et al., 1998; Z. Xu et al., 2015). The Sagaing fault separates the Indochina continental fragment from the Burma block (Figure 1; Akciz et al., 2008; Lin et al., 2009; Metacalfe, 2013; Replumaz & Tapponnier, 2003; Y. J. Wang et al., 2006).

The Tengchong block is dominated by volcanic rocks of late Miocene to Holocene age (Figures 2 and 3a; Y. Wang et al., 2007; Zhao & Chen, 1992; Zhu et al., 1983; Zou et al., 2010), although magmatism was active since Mesozoic times (Dong et al., 2006; H. Li et al., 2011). Widely exposed Pliocene-Holocene volcanics of the Tengchong field are mainly distributed along NE-NNE trending basins, alternated with Mesozoic granites and sedimentary strata. The distribution of upper Cenozoic volcanic rocks covers an area of 792 km^2. Volcanic centers are located within a 90 km long and 50 km wide N-S trending graben. There are 68 late Neogene-Quaternary volcanic centers, 145 hot springs, and 25 preserved volcanic craters and cones (C. Jiang, 1998; C. Jiang et al., 2003). Pliocene-Holocene volcanic activity of the Tengchong field can be grouped into at least three different types (C. Jiang, 1998; D. M. Li, Li, & Chen, 1999): (1) Middle-Upper Pliocene to Upper Pleistocene basalts, (2) Lower Pleistocene silicic pyroclastic rocks, and (3) Holocene basaltic andesites (D. M. Li et al., 1999; Mu et al., 1987; F. Wang et al., 1999; Zou et al., 2014). Further south, the Mangbang basin was interpreted as a half graben developed along the Gaoligong shear zone. It is filled of upper Miocene-Pliocene sandstones and mudstone intercalated with tuffs and basalts (Figure 2; G. Wang et al., 2008).

Volcanics from the Tengchong field and the Mangbang basin were dated by whole rock K-Ar (C. Jiang, 1998; D. Li, Li, & Chen, 2000; Mu et al., 1987) and zircon U-Th-Pb geochronology (Tucker et al., 2013; Zou et al., 2010), yielding 0.87 to 0.01 Ma ages for the Tengchong field and 7.2 to 1.4 Ma ages for the Mangbang field. Volcanism is considered to be locally active (Tucker et al., 2013).

To the east of the Gaoligong shear zone, continuous marine and nonmarine successions are exposed in the Baoshan block. The deformed marine sediments consist of Upper Proterozoic to Triassic carbonates, sandstones, siltstones, and shales deposited in a platform environment. The continental deposits are made of Jurassic-lower Cenozoic red beds (Figure 2; Huang et al., 2015; E. Q. Wang & Burchfiel, 1997).

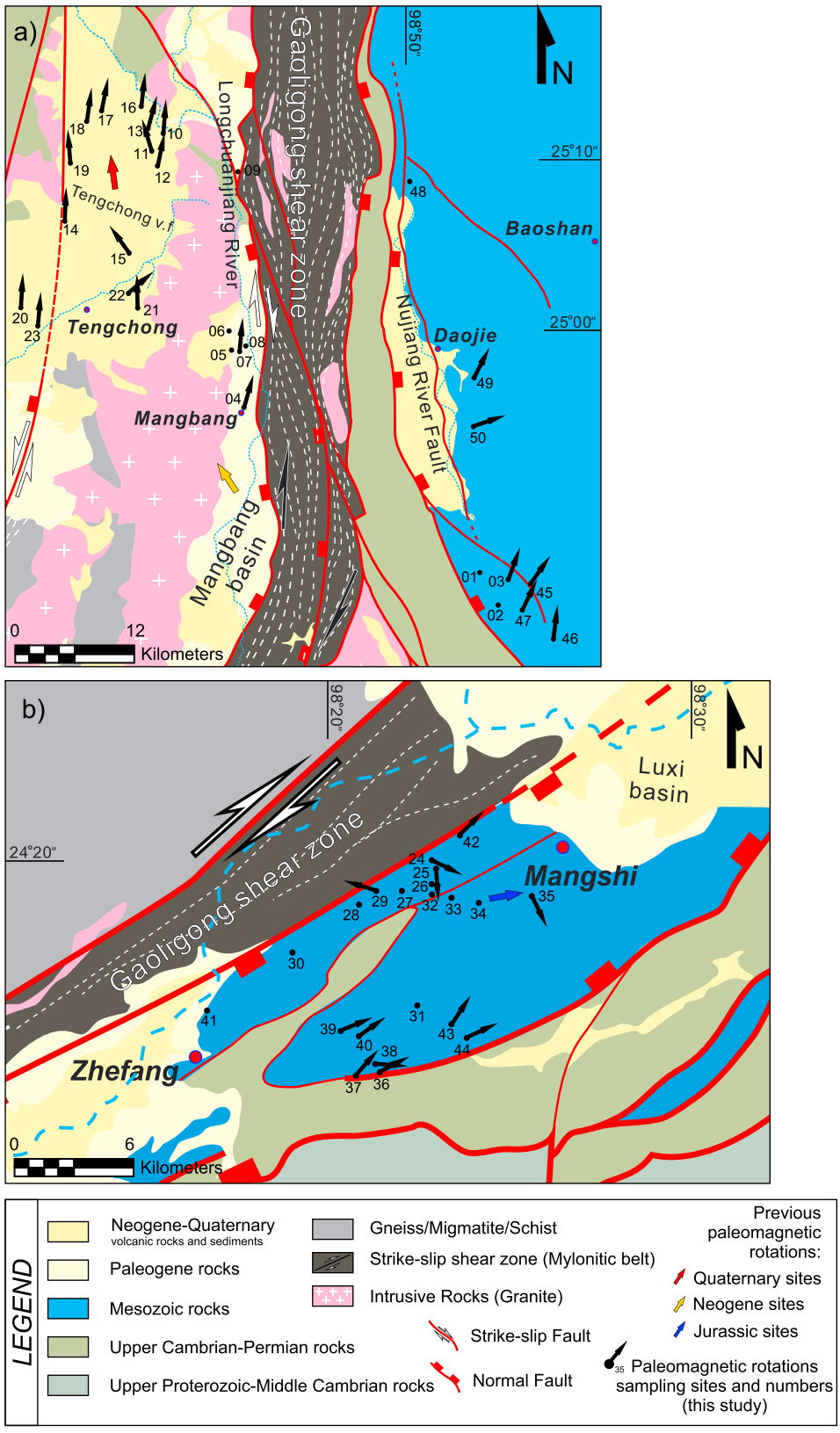

Figure 3. Paleomagnetic sampling areas in the northern (a, Baoshan and Tengchong area) and southern (b, Mangshi basin) segment of the Gaoligong shear zone. Black arrows indicate paleomagnetic rotations from Jurassic to Holocene sediments and basalts (see Table 2). Rotation values were calculated with the same method and Eurasian poles as in Figure 1.

Rare upper Eocene-Oligocene conglomerates and sandstones rest unconformably on older rocks and may have been deposited during regional shortening and strike-slip deformation (E. Q. Wang & Burchfiel, 1997). Pliocene volcanic and sedimentary rocks, and Pleistocene strata are mostly undeformed (E. Q. Wang & Burchfiel, 1997). Cenozoic rocks were involved in intensive shortening along a number of N-S trending folds and thrust faults, which are narrow and merge with each other at the northern end of the Baoshan block. The Baoshan block is bounded to the south by the active left-lateral Nantinghe fault (Figure 1; Socquet & Pubellier, 2005): seismicity and stream offset analysis indicate that this fault may accommodate at present a 1 mm/year deformation rate (Laccassin et al., 1998).

5. Previous Paleomagnetic Data

A wealth of paleomagnetic data has been gathered during the last decades from Yunnan. Here all the previously obtained rotations were recalculated using updated 170–140 Ma Eurasian and 130–10 Ma East Asia reference poles from Torsvik et al. (2012) and Cogné et al. (2013), respectively (Figure 1 and Table 1).

Previous paleomagnetic evidence indicates that rotation of crustal fragments in this region was not homogeneous, likely due to crustal heterogeneity and spatial and temporal stress field variations (S. Li, Advokaat, et al., 2017; Metcalfe, 2002, 2011; Yin & Harrison, 2000).

Only Huang and Opdyke (1991) and Ali et al. (2013) reported data from Permian basalts of the Baoshan Block, reconstructing their former position within the Gondwana supercontinent. In turn, several paleomagnetic works (synthetized by Otofuji et al., 2010) were conducted between 1993 and 2009 on the Jurassic-upper Cretaceous red beds exposed in the Lanping-Simao block, between the Ailao Shan-Red River and Chongshan shear zone. The data show variable yet predominant CW rotations up to 132° with respect to Eurasia. The southward drift of ~1,000 km during the last 50 Ma proposed by Tong et al. (2013) was recently dismissed by S. Li, Advokaat, et al. (2017), who proved that low paleomagnetic inclinations are instead due to sedimentary "inclination flattening" process (e.g., Tauxe, 2005).

Cretaceous and Jurassic red beds have been paleomagnetically studied in south and southwest Yunnan (Huang & Opdyke, 1993), and the rotation pattern revealed that the Xiaguan area did not rotate with respect to stable Eurasia since Late Cretaceous times, and that the Jinggu-Mengla area rotated CW by 46°–65°. Furthermore, in the Yunlong area, about 50 km west of the Ailao Shan-Red River shear zone, Sato et al. (1999) and Yang et al. (2001), documented CW rotations and inferred that Indochina was squeezed out of the Asian continent due to collision of India, accompanied with CW rotations. Similar evidence was found from Lower Cretaceous sites near the city of Yongping. Data show a CW rotation of 25° ± 16°, associated with rotation of the Yongping (Funahara et al., 1993).

In the northern Simao block, Chen et al. (1995) documented CW rotations $>$90°, 77°, and 15° in Lower Cretaceous, Eo-Oligocene, and Miocene sediments (respectively) from the Jinggu area. The available Cretaceous paleomagnetic data from the Jinggu area and neighboring regions demonstrate variable rotations in different sampling localities, possibly bounded by strike-slip faults. This would imply that the Yunnan region and surrounding areas were not deformed as a coherent block in response to the collision of India with Asia (Chen et al., 1995).

Sato et al. (2007) investigated Cretaceous red sandstones and siltstones in Pu'er, northern part of the Simao block, finding a 46° ± 9° CW rotation, which is consistent with the large rotations in the Mengla and Jinggu areas (47° and 66°). The CW rotation of the northern part of the Simao block is larger by more than 20° compared to the Yunlong and Yongping areas belonging to the Lanping block (Sato et al., 2001). Geological, geochronological, and GPS data, obtained from the Lanping-Simao block, seem to demonstrate the close relationship between the Lanping-Simao arcuate structural zone and differential tectonic rotations (Kondo et al., 2012; Tanaka et al., 2008; Tong et al., 2013).

Recently, S. Li, Yang, et al. (2017) focused on Paleocene-Oligocene redbeds and mid-Miocene silts from the Jinggu Basin, northern Simao block. Although a prefolding magnetization was proved in red beds, exclusively normal polarity sites were documented (consistently with previous evidence by Chen et al., 1995; Gao et al., 2015; Huang & Opdyke, 1993). Thus, S. Li, Yang, et al. (2017) concluded that either the studied strata were in fact deposited during the long normal Cretaceous superchron, or the red beds underwent a widespread

prefolding Tertiary overprint. In any case, red beds yield greatly variable CW rotations (ranging from 0° to >90°) that S. Li, Yang, et al. (2017) average to a 30° value, while mid-Miocene sediments do not rotate.

Kornfeld, Eckert, Appel, Ratschbacher, Pfänder, et al. (2014) documented a 40° CW rotation in 30 Ma basalts from the Baoshan block, while Kornfeld, Eckert, Appel, Ratschbacher, Sonntag, et al. (2014) found an 87° CW rotation in 40 Ma dykes from the Tengchong block (Table 1). Counterclockwise (CCW) paleomagnetic rotations reported by Kornfeld, Sonntag, et al. (2014) from lower Pliocene to Holocene volcanics of the Mangbang basin were interpreted as apparent rotations due to tilting around horizontal axes along listric normal faults cutting the Tengchong volcanic field. Finally, Tong et al. (2016) studied Paleocene-Oligocene red beds located at the center of the Baoshan block, NE of Yongde (Figure 1). A primary magnetization was isolated in the Paleocene sediments, while the Eocene-Oligocene red beds were found to be magnetically overprinted during the Miocene. In any case, both localities and sedimentary sequences yielded significant CW rotations, ranging from 70° to 80° (Table 1).

6. Paleomagnetic Sampling and Methods

We collected 503 paleomagnetic samples from 50 sites (Figures 2 and 3), located within a maximum distance of ~25 km from the contact with the Gaoligong shear zone mylonites, and at both sides of it (Figure 2). Such distance was established considering that several studies demonstrated that shear-related rotations virtually end within 10–20 km from fault trace (Hernandez-Moreno et al., 2014; Piper et al., 1997; Randall et al., 2011; Ron et al., 1984; Sonder et al., 1994).

Sites were selected from three main areas to the west, east, and south of the Gaoligong shear zone, in the Tengchong, Baoshan, and Mangshi areas, respectively (Figures 3a and 3b). We gathered 15 paleomagnetic sites in Pliocene-Holocene lavas, 2 sites in Jurassic basalts, 5 sites in Pliocene whitish lacustrine siltstones, and 28 sites in Jurassic-Cretaceous continental red beds, typically made of red fine-grained sandstone or siltstone (Figures 2 and 3 and Table 2). Bedding of Jurassic basalts was inferred considering the attitude of neighbor sediments, forming continuous volcano-sedimentary sequences according to available geological maps. In volcanic sites, several samples were gathered in the same flow, while samples from sedimentary sites were spread as much as possible on a given outcrop to try to average out the paleosecular variation (PSV) of the geomagnetic field. Each volcanic site is expected to record an almost instantaneous geomagnetic direction, so that PSV is surely not averaged out within the 17 sites from Pliocene-Holocene and Jurassic basalts.

The samples were drilled using a petrol-powered portable drill cooled by water and oriented in situ using the Sun (when possible) and a magnetic compass, corrected for the local magnetic declination for year 2016 (between 0° and 0.9°W according to National Oceanic and Atmospheric Administration's National Geophysical Data Center, http://www.ngdc.noaa.gov/geomag/declination.shtml). Afterward, the cores were cut into standard cylindrical paleomagnetic specimens of 22 mm height.

Paleomagnetic measurements were carried out in the shielded room of the paleomagnetic laboratory of the Istituto Nazionale di Geofisica e Vulcanologia (Roma), using a 2G Enterprises direct current superconducting quantum interference device cryogenic magnetometer.

Neogene volcanic samples were demagnetized in 10 steps by alternating field (AF) yielded by three orthogonal coils in line with the magnetometer up to a maximum AF peak of 100 mT. Red beds, Jurassic basalts, and whitish siltstones samples were thermally demagnetized using a Pyrox shielded oven in 12 steps of temperature up to 680°C. Demagnetization data were plotted on orthogonal vector component diagrams (Zijderveld, 1967).

The magnetization components were identified by principal component analysis (Kirschvink, 1980), and the site-mean paleomagnetic directions were computed using Fisher (1953) statistics and plotted on equal-angle projections. Finally, the rotation and flattening values with respect to Eurasia were evaluated according to Demarest (1983), using the reference Eurasia paleopoles by Torsvik et al. (2012) for 170–140 Ma sites and the most recent East Asia-focused poles by Cogné et al. (2013) for 130 to 10 Ma sites. To define the sense and amount of rotation, we always considered the smaller angle between the observed and expected declinations, thereby calculating rotation values always $\leq|180°|$. This is a conservative approach, although we are

Tectonics

10.1029/2017TC004899

Table 2
Paleomagnetic Site-Mean Directions From the Gaoligong Shear Zone (Yunnan, China)

Site	Geographic coordinates		Rock type	Series/ epoch	Numerical age (Ma)	Considered palepoles age (Ma)	Bedding (deg)	*n*/*N*	ChRM/high-temperature component				*k*	α_{95} (deg)	*R* (deg)	Δ*R* (deg)	*F* (deg)	Δ*F* (deg)
									In situ		Tilt corrected							
	Latitude (°N)	Longitude (°E)							*D* (deg)	*I* (deg)	*D* (deg)	*I* (deg)						
Yun01[a]	24.7760824	98.9282752	Basalts	MJ	163–174	170	80/20	10/10	52.6	−51.0	31.8	−67.1	39.3	7.8	−166.5	16.6	−6.44	6.8
Yun02[a]	24.7437355	98.9482315	Basalts	MJ	163–174	170	80/20	5/10	27.9	10.6	29.1	−1.9	298.5	4.4	−169.2	5.9	58.7	4.6
Yun03	24.7694685	98.9593802	Red beds	MJ	163–174	170	42/50	7/10	346.9	81.4	33.5	34.8	40.3	9.6	15.2	10.3	25.8	8.1
Yun04	24.9399358	98.6699462	Basalts	LP/UP	3.6	—	—	8/8	196.3	−37.9	—	—	164.8	4.3	16.3	−6.1	5.1	4.3
Yun05	24.9971886	98.6553678	Whitish siltstones	LP	3.6–5.3	—	—	—	—	—	—	—	—	—	—	—	—	—
Yun06	25.015892	98.6535897	Whitish siltstones	LP	3.6–5.3	—	—	—	—	—	—	—	—	—	—	—	—	—
Yun07	24.9967763	98.6658433	Whitish siltstones	LP	3.6–5.3	—	—	6/10	5.8	31.4	—	—	13.7	18.8	5.8	22.1	11.6	18.8
Yun08	24.9977035	98.6675056	Whitish siltstones	LP	3.6–5.3	—	—	—	—	—	—	—	—	—	—	—	—	—
Yun09	25.1686698	98.668388	Whitish siltstones	LP	3.6–5.3	—	—	—	—	—	—	—	—	—	—	—	—	—
Yun10	25.2115518	98.5821019	Basalts	LP/UP	3.6	—	—	10/10	4.6	20.0	—	—	163.3	3.8	4.6	4.1	23.0	3.8
Yun11	25.194456	98.5693205	Basalts	LPS	1.5–2.5	—	—	9/10	343.5	22.5	—	—	53.5	7.1	−16.5	7.7	20.5	7.1
Yun12	25.1795786	98.5758987	Basalts	LPS	1.5–2.5	—	—	10/10	12.2	47.1	—	—	40.3	7.7	12.2	11.3	−4.1	7.7
Yun13	25.213207	98.5749002	Basalts	LP/UP	3.6	—	—	10/10	15.5	35.1	—	—	184.4	3.6	15.5	4.4	7.9	3.6
Yun14	25.1249219	98.4719548	Basalts	H	Present–0.0117	—	—	9/11	2.9	24.4	—	—	261.3	3.2	2.9	3.5	18.6	3.2
Yun15	25.0935656	98.5443339	Basalts	LPS	1.5–2.5	—	142/67	10/10	324.7	20.2	—	—	20.8	10.8	−35.3	11.6	22.8	10.8
Yun16	25.238754	98.5577044	Basalts	H	Present to 0.0117	—	149/10	10/10	6.8	34.7	12.0	42.3	176.6	3.6	6.8	4.4	8.3	3.6
Yun17	25.234284	98.5142608	Basalts	H	Present to 0.0117	—	—	9/11	11.5	35.0	—	—	89.9	5.5	11.5	6.8	8.0	5.5
Yun18	25.2238856	98.4980389	Basalts	H	Present to 0.0117	—	—	10/11	8.3	33.7	—	—	46.9	7.1	8.3	8.6	9.3	7.1
Yun19	25.1826527	98.4799935	Basalts	H	Present to 0.0117	—	—	9/10	356.0	16.9	—	—	84.3	5.6	−4.0	5.9	26.1	5.6
Yun20	25.0393686	98.4258614	Basalts	H	Present to 0.0117	—	—	9/10	3.7	28.5	—	—	297.0	3.0	3.7	3.4	14.5	3.0
Yun21	25.0406369	98.5537038	Basalts	LPS	1.5 to 2.5	—	—	10/10	179.1	−42.8	—	—	63.7	6.1	−0.9	8.4	0.2	6.1
Yun22	25.0521541	98.5450541	Basalts	LPS	1.5 to 2.5	—	—	10/11	230.0	−47.3	—	—	50.5	6.9	50.0	10.3	−4.3	6.9
Yun23	25.0208672	98.4448747	Basalts	H	Present to 0.0117	—	294/10	10/10	5.2	29.2	0.3	25.5	92.5	5.1	5.2	5.9	13.8	5.1
Yun24	24.3443875	98.3921232	Red beds	K	66–145	**100**	230/12	9/12	299.8	−17.2	303.8	−21.0	19.1	12.1	115.8	10.5	17.7	10.2
Yun25	24.3405986	98.3929158	Red beds	J-K	66–201	160	185/59	7/12	165.5	−72.7	13.4	−47.1	10.1	20.0	176.2	24.0	9.4	16.0
Yun26	24.3347198	98.394079	Red beds	K	66–145	—	—	—	—	—	—	—	—	—	—	—	—	—
Yun27	24.331493	98.3774904	Red beds	K	66–145	—	—	—	—	—	—	—	—	—	—	—	—	—
Yun28	24.32577171	98.35766892	Red beds	K	66–145	—	—	—	—	—	—	—	—	—	—	—	—	—
Yun29	24.33141523	98.36594508	Red beds	K	66–145	**100**	164/75	9/11	302.9	−21.1	294.8	35.9	10.7	16.5	−73.7	16.3	12.6	13.2
Yun30	24.3064965	98.3273209	Red beds	K	66–145	—	—	—	—	—	—	—	—	—	—	—	—	—
Yun31	24.2846044	98.3841427	Red beds	MJ	163–174	—	—	—	—	—	—	—	—	—	—	—	—	—
Yun32	24.3316463	98.393859	Red beds	K	66–145	—	—	—	—	—	—	—	—	—	—	—	—	—
Yun33	24.32879722	98.39939239	Red beds	MJ	163–174	—	—	—	—	—	—	—	—	—	—	—	—	—
Yun34	24.3266414	98.41226722	Red beds	MJ	163–174	—	—	—	—	—	—	—	—	—	—	—	—	—
Yun35	24.3294147	98.4357429	Red beds	J-K	66–201	160	323/43	5/10	351.3	18.2	351.6	−20.0	86.8	8.3	154.4	8.5	36.6	7.5
Yun36	24.255107	98.3670267	Red beds	MJ	163–174	160	346/44	9/10	108.3	25.1	80.0	40.0	70.2	6.2	62.7	8.0	16.6	6.2
Yun37	24.2530733	98.3559025	Red beds	MJ	163–174	160	327/75	9/10	92.8	7.6	58.6	36.5	106.7	5.0	41.2	6.9	19.8	5.5
Yun38	24.2588832	98.361492	Red beds	MJ	163–174	160	335/44	6/10	118.6	−4.6	111.9	30.0	14.8	18.0	94.7	17.0	26.5	15.5
Yun39	24.2737808	98.3497701	Red beds	MJ	163–174	160	165/23	8/8	70.7	32.3	85.1	30.9	17.0	13.8	67.9	13.5	25.6	11.4
Yun40	24.2716601	98.3572075	Red beds	MJ	163–174	160	135/88	8/10	21.5	25.5	71.8	22.0	14.3	15.1	54.6	13.7	34.5	12.4
Yun41	24.2826614	98.28916	Red beds	K	66–145	—	—	—	—	—	—	—	—	—	—	—	—	—
Yun42	24.3547169	98.40384259	Red beds	K	66–145	**100**	160/38	5/5	14.0	38.1	53.1	62.6	51.7	10.7	45.1	18.8	−23.9	9.2
Yun43	24.2767445	98.3995939	Red beds	MJ	163–174	160	331/52	7/10	87.8	29.0	50.8	37.5	41.1	9.5	33.6	10.6	19.0	8.3
Yun44	24.2710038	98.4064307	Red beds	MJ	163–174	160	5/44	10/10	110.1	30.2	82.3	31.2	69.3	5.8	65.1	7.3	25.3	5.9
Yun45	24.7620875	98.985785	Red beds	MJ	163–174	160	65/84	9/10	260.8	52.7	52.3	41.5	15.7	13.4	34.6	14.9	15.0	11.1
Yun46	24.7103859	99.0088921	Red beds	MJ	163–174	160	81/22	9/10	6.9	44.2	23.8	35.0	19.7	11.9	6.6	12.4	22.0	10.0
Yun47	24.7390466	98.9747164	Red beds	MJ	163–174	160	69/50	10/10	319.5	70.3	42.9	43.7	45.8	7.2	25.7	9.3	13.4	6.8

Table 2 *(continued)*

Site	Geographic coordinates		Rock type	Series/ epoch	Numerical age (Ma)	Considered paleopoles age (Ma)	Bedding (deg)	ChRM/high-temperature component										
									In situ		Tilt corrected							
	Latitude (°N)	Longitude (°E)						*n/N*	*D* (deg)	*I* (deg)	*D* (deg)	*I* (deg)	*k*	α_{95} (deg)	*R* (deg)	ΔR (deg)	*F* (deg)	ΔF (deg)
Yun48	25.1643668	98.8513117	Red beds	MJ	163–174	—	—	—	—	—	—	—	—	—	—	—	—	—
Yun49	24.9697763	98.9220494	Red beds	MJ	163–174	160	76/70	10/10	310.8	58.1	44.2	35.2	29.0	9.1	27.0	10.1	22.0	8.0
Yun50	24.9209456	98.9212281	Red beds	MJ	163–174	160	127/47	10/10	341.1	63.1	94.3	61.9	32.7	8.6	77.1	15.3	−4.6	7.7

Note. Ages: J = Jurassic; MJ = Middle Jurassic; K = Cretaceous; LP = Lower Pliocene; UP= Upper Pliocene; LPS = Lower Pleistocene; H = Holocene. The geographic coordinates are referred to WGS84 datum. Age in Ma is from the geologic timescale of Cohen et al. (2013). Bedding is expressed in dip azimuth/dip values. *D* and *I* are site-mean declination and inclination calculated before and after tectonic correction; *k* and α_{95} are statistical parameters after Fisher (1953); *n/N* is number of samples giving reliable results/number of studied samples at a site. Site-mean rotation *R* and flattening *F* values, and relative errors ΔR and ΔF (according to Demarest, 1983) are relative to coeval *D* and *I* Eurasian values expected at the sampling area considering Eurasian paleopoles from Torsvik et al. (2012) and Cogné et al. (2013) (in bold). *R* and *F* for Holocene sites were evaluated comparing the paleomagnetic directions with local geocentric axial dipole field direction.
[a]Discarded site (see text).

aware that in the past, some authors considered rotation values exceeding 180° (e.g., Hernandez-Moreno, et al., 2014 and references therein).

Moreover, for each sampling site, we selected specimens for additional magnetic mineralogy analyses. For hysteresis measurements, the samples were crushed into powder and placed in pharmaceutical gel caps #4 (filled volume ~0.15 ml), in order to vibrate by means of a carbon fiber probe in the Princeton Measurement Corporation Micromag 3900 vibrating sample magnetometer. The coercive force (Bc), the saturation or maximum remanent magnetization (Mrs), and the saturation/maximum magnetization (Ms) were measured using the vibrating sample magnetometer under cycling in a maximum field of 1.0 T and determined after subtracting the high field paramagnetic linear trend when saturated samples. The coercivity of remanence (Bcr) values have been extrapolated from the backfield remagnetization curves up to −1 T, following a forward magnetization in +1 T field. Bcr represents the negative field needed to remove the remanent magnetization after applying the maximum positive field. The saturation remanence to saturation magnetization (Mrs/Ms) versus the ratio of remanent coercive force to coercive force (Bcr/Bc) has been plotted in a "Day plot" (Day et al., 1977; Dunlop, 2002).

First-order reversal curves (FORCs) have been measured using the Micromag operating software and processed, smoothed, and drawn with the FORCINEL Igor Pro routine (R. J. Harrison & Feinberg, 2008). FORCs are a series of partial hysteresis loops made after the sample magnetization is saturated (Pike et al., 1999; Roberts et al., 2000). Selected FORCs have been measured in steps of 2 mT with an averaging time of 100 ms; the maximum applied field was 1.0 T. The optimum smoothing factor was calculated by the FORCINEL software.

For one specimen from each basalt site we also measured the variation of the low-field magnetic susceptibility (κ) during a heating and cooling cycle performed in air, from room temperature up to 700°C, using an AGICO KLY-3 Kappabridge coupled with a CS-3 furnace. The Curie/Néel points have been estimated as the temperature, or range of temperatures, at which the paramagnetic behavior starts to dominate, following the approach outlined by Petrovský and Kapička (2006).

7. Magnetic Mineralogy Results

The magnetic mineralogy of the samples is heterogeneous (Figure S1 in the supporting information), ranging from almost paramagnetic (whitish siltstones sites Yun05 to Yun09 and red beds site Yun32) to prevailing low coercivity and saturated at low field properties (Pliocene-Holocene basalt sites Yun04, Yun11 to Yun16, Yun18 to Yun23, and red beds sites Yun33 to Yun34), up to high coercivity and/or markedly unsaturated features at 1 T (Jurassic basalt sites Yun01 and Yun02 and red beds sites Yun03, Yun24 to Yun31, Yun35 to Yun50).

The main ubiquitous magnetic minerals are magnetite/titanomagnetite in the volcanics and hematite in the red beds; the magnetic susceptibility versus temperature curves show that hematite is also present in the low coercivity class of samples, considering that κ does not completely drop before 680°C (Figure S1). In this case, the presence of hematite in the thermomagnetic curves can also be ascribed to the inversion of ferromagnetic maghemite occurring from $T > 350$°C. For most of the samples, cooling curves are below the heating curves, thus excluding the relevant formation of ferrimagnetic minerals while heating in air.

The Day plot has been drawn only for the low coercivity/saturated samples, in order to define the domain state and the consequent magnetic grainsize according to the theoretical hysteresis ratios expected for magnetite and titanomagnetite (Figure S1).

Most of these samples fall in the upper-central region of the plot, not far from the upper segment of the theoretical curves calculated for mixtures of single domain (SD) and multidomain (MD) magnetite grains, thus suggesting a significant contribution of stable SD particles to the overall magnetic mineralogy.

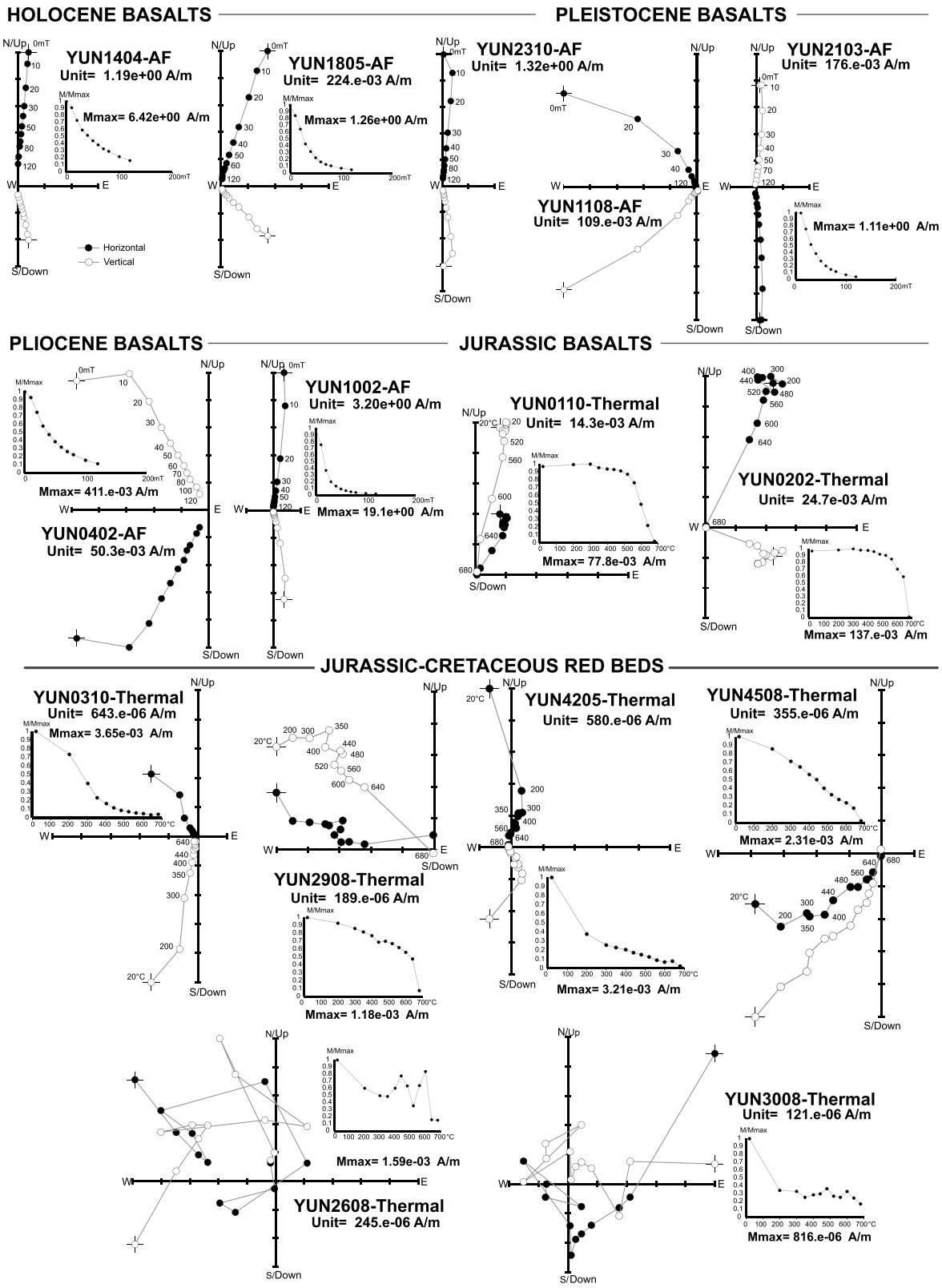

Figure 4. Orthogonal vector diagrams of typical demagnetization data (in situ coordinates) showing representative samples carrying characteristic magnetization components (ChRMs), low/high temperature components (Yun2908, Yun4508), and scattered magnetization (Yun2608, Yun3008). Solid (open) symbols represent projection onto the horizontal (vertical) plane. Demagnetization step values are in milli Tesla (mT) and degrees Celsius for the alternating field and thermally demagnetized samples, respectively.

Noteworthy, selected samples from volcanic sites Yun10, Yun14, and Yun17 show wasp-waisted hysteresis loops, which can be ascribed both to the coexistence of superparamagnetic (SP) and single-domain (SD) particles or to the mixing of hard and soft coercivity magnetic minerals, as magnetite and hematite (Roberts et al., 1995).

The FORC diagram of a selected sample from site Yun10 shows closed contours peaked at about 15–20 mT, with a concurring secondary peak at the origin and asymmetric nearly vertical contours extending into the lower quadrant (Pike et al., 2001), thus indicating that the wasp-waisted shape of the hysteresis loop, in this case, is due to the coexistence of ultrafine SP and fine SD magnetite particles.

8. Paleomagnetic Results and Magnetic Overprint Evaluation

Thirty-five (18 Jurassic-Cretaceous red beds, 2 Jurassic basalts, and 15 Pliocene-Holocene basalts) out of 50 sites gave reliable paleomagnetic results, the remaining 15 sites yielded erratic demagnetization diagrams and were discarded from further consideration. All Pliocene lacustrine siltstone samples, except site Yun07, gave not-interpretable diagrams.

In the AF demagnetized volcanic rocks, a viscous component was removed between 10 and 30 mT, and a characteristic magnetization (ChRM) was isolated between 30 and 120 mT (Figure 4), confirming the occurrence of magnetite and titanomagnetite. In the thermally demagnetized Jurassic basalts, a ChRM was isolated between 480 and 680°C. In the red beds samples, after the elimination of a viscous component up to 200°C, a ChRM was isolated in about half of the samples between 200 and 680°C. In the remaining samples, a low- and high-temperature (HT) components were defined in the 200–400°C and 400–680°C intervals, respectively (sample Yun2908 in Figure 4). The high unblocking temperature spectra and Curie temperature of 680°C combined with high coercivity spectra show that hematite is the main magnetic carrier in the red beds (confirming evidence from previous paleomagnetic studies from Yunnan, e.g., Sato et al., 2007; Tong et al., 2013, 2016). Several studies carried out over nearly the last 50 years have showed that hematite in red beds may have both a detrital and a chemical origin (see review by Z. Jiang et al., 2015).

By combining ChRMs and HT components, well-defined site-mean directions ($3.0° \leq \alpha_{95} \leq 20.0°$, 9.1° on average) were obtained from 15 Pliocene-Holocene volcanic sites, 1 Pliocene lacustrine site, 18 Jurassic-Cretaceous red bed sites, and 2 Jurassic volcanic sites (Table 2).

In Figure 5, we show the paleomagnetic site-mean directions from Pliocene-Holocene basalts from our work (Figure 5a) and Eocene-Pliocene volcanics sampled in neighbor regions by Kornfeld, Eckert, Appel, Ratschbacher, Pfänder, et al. (2014), Kornfeld, Eckert, Appel, Ratschbacher, Sonntag, et al. (2014), and Kornfeld, Sonntag, et al. (2014; Figures 5b–5d). Our data and those by Kornfeld, Sonntag, et al. (2014) come from the same rocks from the Tengchong volcanic field, so that they should compare. The results are effectively the same (considering respective confidence cones) and show mostly northward declinations in the Tengchong volcanic field. Our data reveal higher inclination with respect to data by Kornfeld, Sonntag, et al. (2014). Moreover, three sites (two Pleistocene and one Pliocene in age) yield reverse polarities and inclinations as high as −37.9° to −47.3°. Therefore, our data demonstrate that the Tengchong volcanic field is older than 0.78 Ma (age of the Brunhes-Matuyama transition; geomagnetic polarity scale from Ogg, 2012), confirming radiometric data by G. Wang et al. (2008, and references therein). The lower inclination with respect to the geocentric axial dipole (GAD) field inclination expected at the study area may be due to the incomplete averaging of the PSV of the geomagnetic field, as we got samples from only 15 lava flows. Thus, we put forward an alternative explanation for the low normal polarity inclinations from the Tengchong volcanic field than the regional tilting proposed by Kornfeld, Sonntag, et al. (2014).

In Figure 5b, we also show data from Kornfeld, Sonntag, et al. (2014) obtained from upper Miocene-Pliocene volcanic rocks of the Mangbang Basin. They explained the CCW rotations as apparent rotations due to tilting along the half graben hosting the basin itself. Kornfeld, Eckert, Appel, Ratschbacher, Pfänder, et al. (2014) also documented a 40° CW rotation in 30 Ma basalts from the Baoshan block (Figure 5c) and a CW rotation of 87° in 40 Ma dykes from the Tengchong block (Figure 5d).

Paleomagnetic directions from Jurassic-Cretaceous red beds sampled east of the Gaoligong shear zone are shown in Figure 6. Site-mean directions were evaluated by averaging out ChRMs and HT components from the individual specimens. Both the in situ and tilt-corrected directions are far from the GAD field direction expected at the

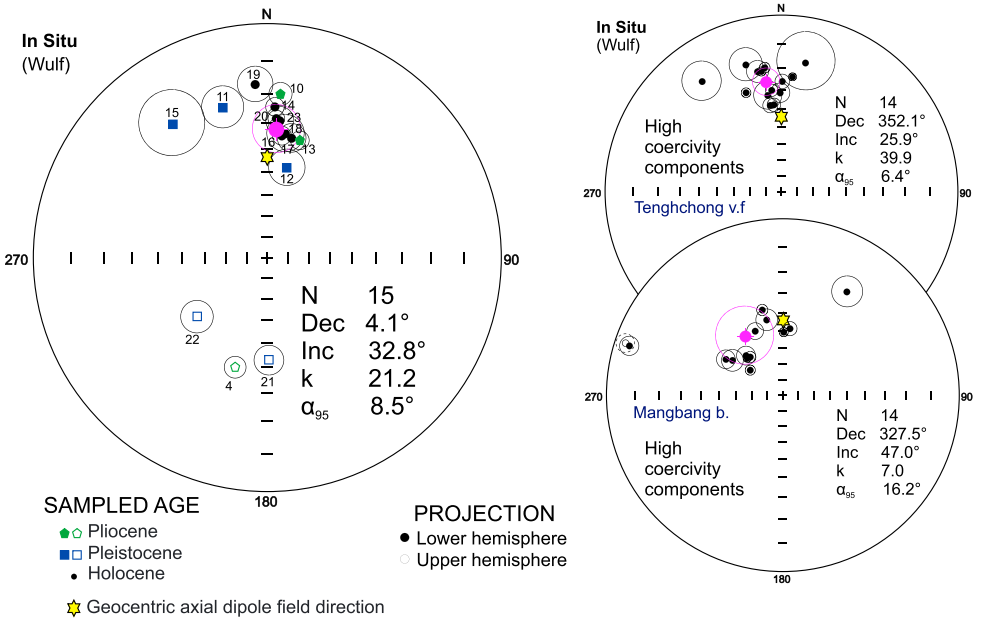

***a.* Data from this work. Basalts, Tengchong volcanic field and city;**

***b.* Data from Kornfeld, Sonntag, et al. (2014) volcanic rocks of the Tengchong volcanic field and Mangbang basin (late Miocene-Pliocene);**

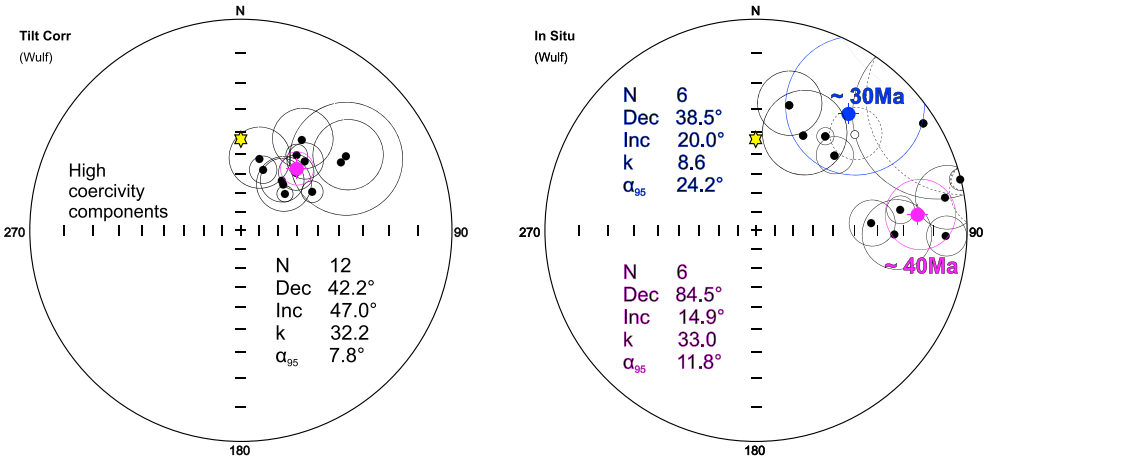

***c.* Data from Kornfeld, Eckert, Appel, Ratschbacher, Pfänder, et al. (2014) volcanic rocks (~ 30-40 Ma) of the Baoshan block;**

***d.* Data from Kornfeld, Eckert, Appel, Ratschbacher, Sonntag, et al. (2014) volcanic rocks of the Tengchong block.**

Figure 5. Equal-angle projection of the site-mean paleomagnetic directions gathered by us from Pliocene-Holocene basalts exposed west of the Gaoligong shear zone (a), and by Kornfeld, Eckert, Appel, Ratschbacher, Pfänder, et al. (2014); Kornfeld, Eckert, Appel, Ratschbacher, Sonntag, et al. (2014); Kornfeld, Sonntag, et al. (2014) (b–d). *N* = number of sites; *Dec* = declination; *Inc* = inclination; *k* = precision parameter; a_{95} = 95% confidence angle. The yellow stars represent the normal polarity geocentric axial dipole field direction (*D* = 0°; *I* = 43°) expected at the study area. Solid (open) symbols represent projection onto the lower (upper) hemisphere, and open circles represent confidence cones. Pink points and open circles represent the mean paleomagnetic directions and the relative 95% confidence cones, respectively.

sampling localities. Most of the tilt corrected directions (15 out of 18 sites) are of normal polarity and show variable amounts of westward declinations (exceeding 100° for site Yun38). Directions from Jurassic volcanics (sites Yun01–Yun02) were discarded, as they were completely different from nearby red bed site directions (Figure 3 and Table 2). Moreover, site Yun02 yielded a subhorizontal tilt-corrected direction that is incompatible with the expected Jurassic inclinations (42°–61°, e.g., Torsvik et al., 2012).

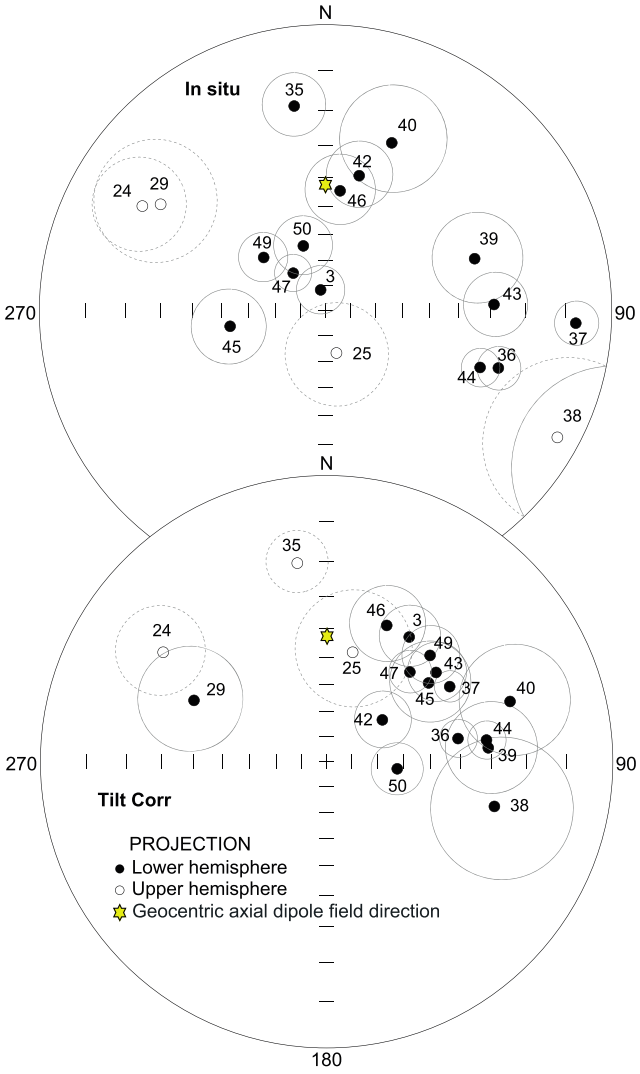

Figure 6. Equal-angle projection of the paleomagnetic directions obtained from Jurassic-Cretaceous red beds exposed in the Baoshan and Mangshi areas, east of the Gaoligong shear zone (see Figure 3).

The paleomagnetic data from red beds support a positive fold test at the 99% significance level according to McFadden (1990) (N = 18; $Scos_{insitu}$ = 11.9; $Scos_{tilt\ corrected}$ = 1.1, critical Scos at the 99% significance level = 6.9). Maximum κ and minimum Scos values are obtained at 93% and 95% of complete unfolding, respectively. This suggests a prefolding (i.e., pre-Eo-Oligocene; Chen et al., 1995) magnetization. Furthermore, site Yun38 showed dual polarity samples (and consistent polarities in the same beds), indicating that the sampled strata encompass different polarity chrons (the reversal test on individual ChRMs according to McFadden & McElhinny, 1990 is indeterminate). This proves that at least for site Yun38, the magnetization is of primary origin. The normal and reverse polarity site-mean directions are not antipodal (negative fold test according to McFadden, 1990), probably due to local block rotations.

It is noteworthy that three sites (Yun24, Yun25, and Yun35) from our red bed data set yield a reverse polarity (and Yun38 dual polarity samples), while previous studies of red beds from the Lanping and Simao blocks systematically reported a normal polarity, for which a magnetic overprint has been suggested (Chen et al., 1995; Gao et al., 2015; Huang & Opdyke, 1993; S. Li, Yang, et al., 2017). Red beds sites Yun24, Yun25, and Yun35 support themselves a positive fold test at the 95% significance level according to McFadden (1990; $Scos_{insitu}$ = 2.6; $Scos_{tiltcorr}$ = 1.8, critical Scos at the 95% significance level = 2.1, maximum κ and minimum Scos values arise at 100% of complete unfolding). Thus our data support for sure a prefolding (i.e., pre-Eo-Oligocene) magnetization of the whole data set, and the reverse polarity sites suggest that magnetization is possibly of primary origin. In this case, most of the studied sites would have been deposited during the long normal Cretaceous superchron. Detailed age evaluation is often problematic in continental sediments, so that the issue of age determination and possible lower Cenozoic prefolding remagnetization of most of the sites remains open at present (see also similar conclusions by S. Li, Yang, et al., 2017 for the Simao block).

Although sites Yun24, Yun25, Yun29, and Yun42 are located at less than 2 km from the contact with the mylonites of the Gaoligong fault, a post-rotation (i.e., post Oligo-Miocene) magnetic overprint is excluded (with the possible exception of site Yun42) by the evidence that both the in situ and tilt-corrected directions are far from the GAD field direction (Figure 6 and Table 2). The apparently puzzling lack of a Neogene magnetic overprint for sites adjacent to mylonites is explained considering that the high-grade rocks were exhumed along an extensional detachment that presumably elided the whole upper crust, juxtaposing high-grade metamorphic rocks and unmetamorphosed sediments (B. Zhang et al., 2011).

9. Rotation Pattern Along the Gaoligong Shear Zone

To evaluate tectonic rotations with respect to Eurasia, the paleomagnetic directions were compared to coeval Eurasian paleopoles from Torsvik et al. (2012) and Cogné et al. (2013). Sites younger than 5 Ma (i.e., Pliocene to Holocene in age) were compared to the local GAD field direction, assuming that no paleomagnetically significant East Asia rotation or drift occurred after 5 Ma. The expected Eurasian declinations and inclinations at Yunnan are shown in Figure 7. Inclination data show rapid changes in the 170–150 Ma time window, followed by contrasting paths when the two paleopole lists are considered. Expected declinations are always positive, although they are significant (around 20°) only at 170–150 Ma, between 140 and 80 Ma they are around 10°–20° and are progressively annulled afterward.

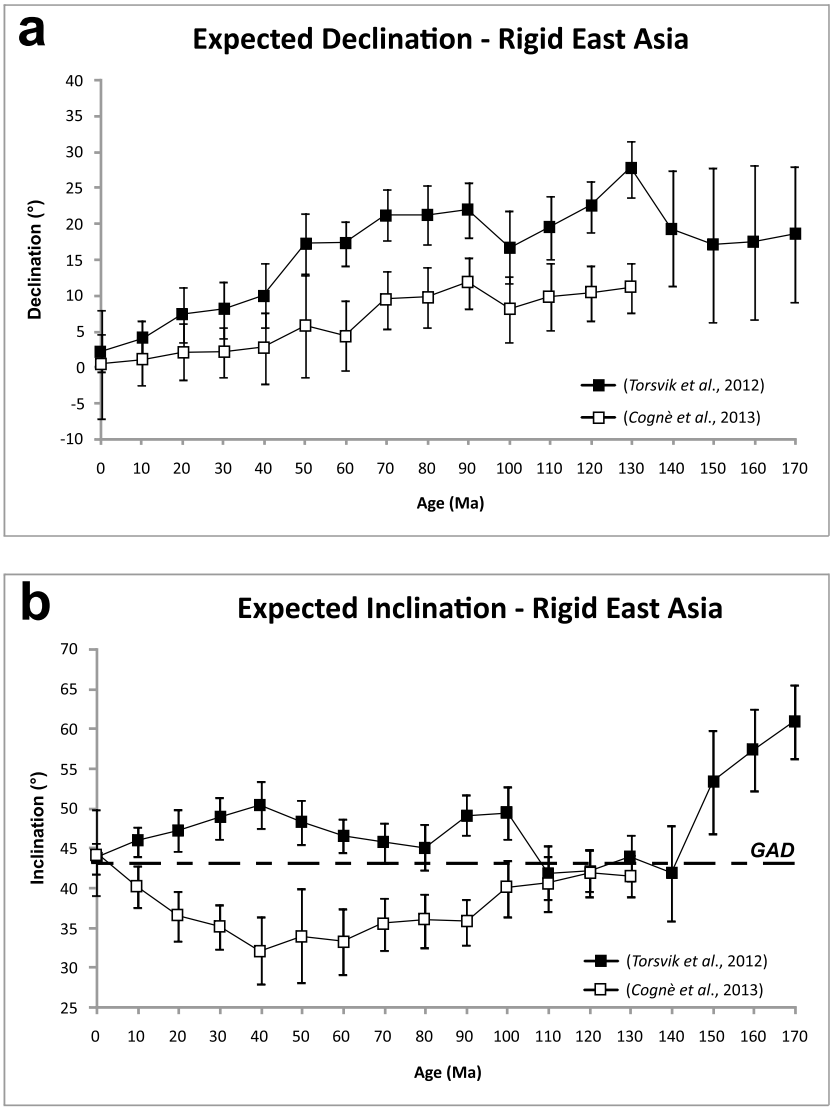

Figure 7. Expected declination and inclination values (and relative error bars) in the study area, considering Eurasian (from 170 to 140 Ma) and East Asia (from 130 to 10 Ma) paleopoles by Torsvik et al. (2012) and Cogné et al. (2013), respectively. Reference point is at 25.21°N, 98.58°E. The black line indicates the geocentric axial dipole field inclination (43°) for the study area.

Site rotations with respect to their distance to the Gaoligong shear zone are shown in Figure 8. Site distances are calculated with respect to both the shear zone center (Figure 8a), and the contact with the fault mylonites (Figure 8b). To the west of the fault, Pliocene-Holocene basalts overall show null rotations, consistently with results from the Pliocene whitish silt site Yun07. As discussed above, PSV from basalt sites is likely not averaged out, and we may expect a geomagnetic declination scatter that mostly ranges within ±20° at such latitudes (Hernandez-Moreno et al., 2016, and discussion therein). Thus, a bias can exist on the average null rotation obtained from volcanic data, but such error is expected to be much smaller than the large CW rotations (up to 176°) observed in Mesozoic red beds. We conclude that data from basalts—although probably scattered by PSV effects—do prove that rotations ceased in Yunnan by Early Pliocene (5 Ma) times. Red beds east of the fault yield always CW rotations (apart from site Yun29), reaching values as high as 176° for site Yun25. Apart for scattered rotations adjacent to the fault (sites Yun24, Yun29, and Yun42), in both plots there is a clear trend of decreasing rotation values moving away from the fault. Rotations are virtually annulled at ~20 km from mylonite-sediment contact (Figure 8b).

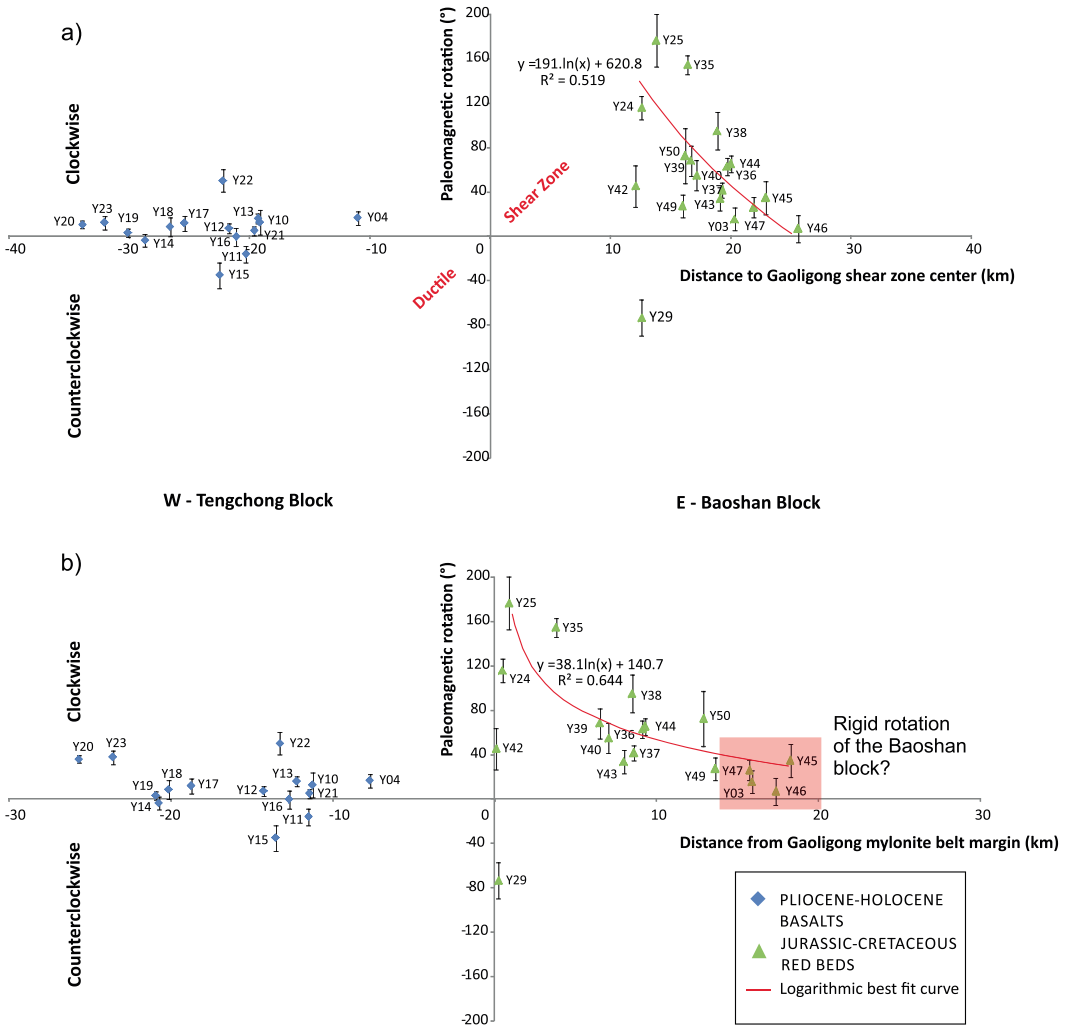

Figure 8. Plot of rotations with respect to Eurasia versus site distance to both Gaoligong shear zone center (a) and mylonite-sediment contact (b). See Figure 3 for site location. Red lines are logarithmic best fit curves for the red bed sites located east of the Gaoligong shear zone (disregarding sites Yun24, Yun29, and Yun42 located adjacent to fault mylonites). Sense and amount of rotation are defined by the smaller angle between observed and expected Eurasian declinations, thus rotation values are $\leq|180°|$ by definition.

There is not clear evidence, in the field, of the width of the rotating blocks. By scrutinizing rotations of sites Yun24, Yun25, Yun29, and Yun42, located adjacent to the Gaoligong shear zone contact (Figure 3b), rotations change abruptly from close sites, suggesting that the crust along the Gaoligong damage zone is broken into small blocks, width in the order of 1 km, or smaller (see sites Yun24 and Yun25). Obviously, block size seems to increase moving away from the fault, and in fact sites located in the southern boundary of the Mangshi basin (Figure 3b) show similar rotations over a distance of 6–7 km.

The described CW paleomagnetic data seem to support a "quasi-continuous" crust deformation model of strike-slip fault zones, where the upper brittle crust is broken into small rigid blocks with sizes smaller than the shear zone width, the rotation is CW (CCW) in regions of dextral (sinistral) shear and gradually increases getting closer to the fault, reaching values $>90°$ (Figure 9c; Hernandez-Moreno et al., 2014, 2016; McKenzie & Jackson, 1983; Nelson & Jones, 1987; Randall, Lamb, & Mac Niocaill, 2011; Sonder et al., 1994).

According to such model, the rotation is not directly driven by fault shear but is a consequence of the angular velocity of the ductile deformation, taking place in the ductile lower crust.

We note that our CW rotation pattern is not consistent with (1) the continuous crust deformation models (where even the brittle upper crust behaves as a viscous fluid and rotations are $\leq 90°$ (Bird & Piper, 1980;

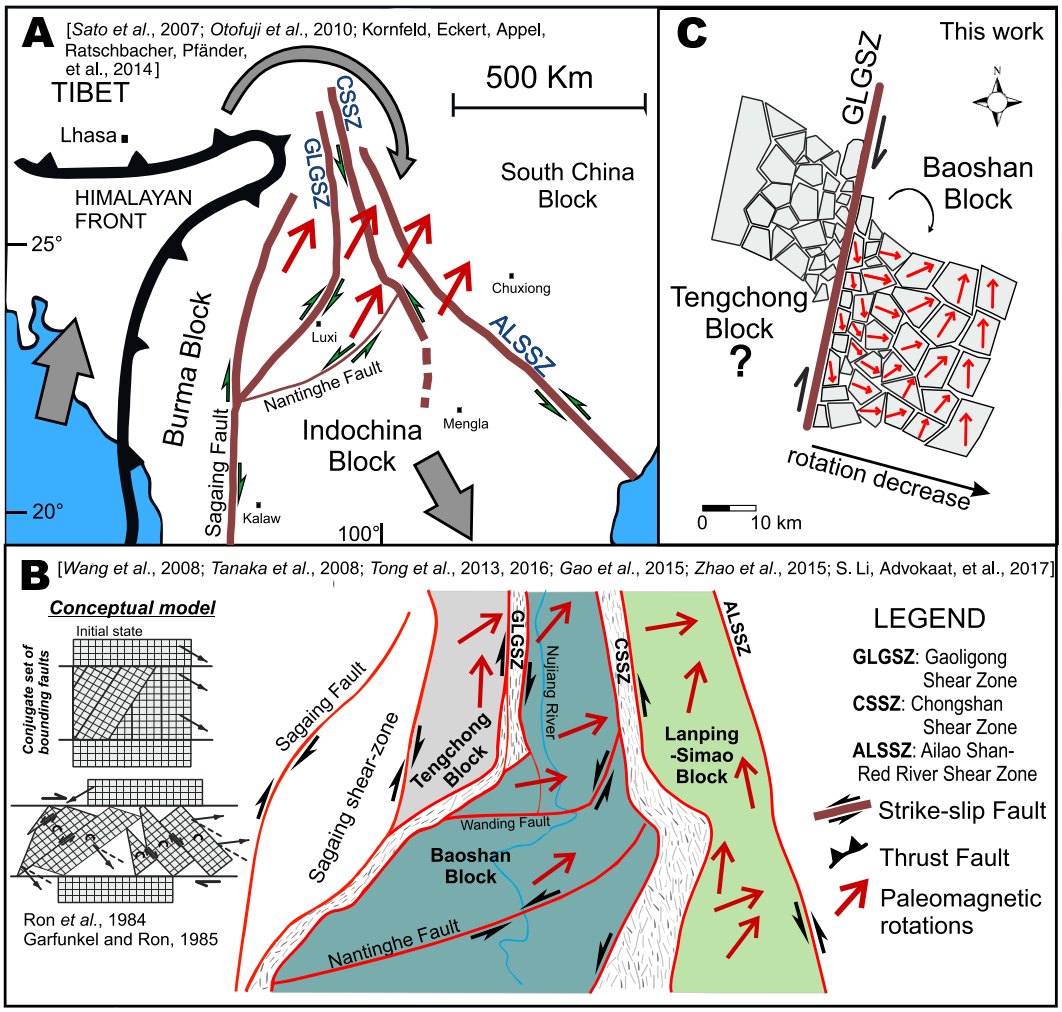

Figure 9. Kinematic models of block rotations proposed for the Yunnan region. (a) Eastward extrusion of the Tibet plateau, yielding clockwise crust rotation around the East Himalayan Syntaxis, and inducing constant-magnitude clockwise rotations in Yunnan (Kornfeld, Eckert, Appel, Ratschbacher, Pfänder, et al., 2014; Otofuji et al., 2010; Sato et al., 2007); (b) rigid mega-block rotations induced by shear along the Gaoligong and adjacent shear zones of Yunnan (similar to "broken slate" model by Ron et al., 1984; Garfunkel & Ron, 1985; Nur et al., 1986). Each block rotates rigidly and is bounded by a major shear zone (Gao et al., 2015; S. Li, Advokaat, et al., 2017; Tanaka et al., 2008; Y. B. Tong et al., 2013; G. Wang et al., 2008; Zhao et al., 2015); c) quasi-continuous block rotation model (e.g., Lamb, 1987; Randall et al., 2011; Sonder et al., 1994; see also Hernandez-Moreno et al., 2014, 2016) for the Tengchong and Baoshan blocks at both edges of the Gaoligong shear zone, based on paleomagnetic rotations reported in this work. Rotations of small blocks of Jurassic-Cretaceous red beds east of the Gaoligong shear zone (Baoshan block) are caused uniquely by dextral shear along the Gaoligong shear zone. Rotations reach maximum values (176°) close to the fault and diminish moving east of it being virtually annulled at ca. 20 km from the shear zone contact. The dimension and shape of individual crustal blocks are speculative, although—relying on rotation value scatter—blocks adjacent to the fault are ≤1 km wide (see Figure 3). Pliocene-Holocene sites located west of the Gaoligong shear zone (Tengchong block) do not rotate, likely because dextral fault activity and its related rotations are older than Pliocene times.

England et al., 1985; England & McKenzie, 1982; England & Wells, 1991; Kimura et al., 2011; Kimura et al., 2004; Sonder & England, 1986; Sonder et al., 1986) or (2) the discontinuous models, where set of secondary faults inside the deforming zone bound large rigid domains that rotate uniformly CW and CCW ≤90° (Garfunkel & Ron, 1985; McKenzie & Jackson, 1986; Nur et al., 1986; Ron et al., 1984).

In quasi-continuous deformation models, the rotation magnitude of the blocks has been assumed to depend upon fault length, displacement amount, fault wall locking, and lithosphere rheology (Piper et al., 1997; Randall et al., 2011; Sonder et al., 1994). The simpler equation by Lamb (1987), which relates fault zone

deformation-rotation width (W) and displacement (D) with the maximum rotation value of equidimensional blocks (Θ) was recently successfully used to infer the displacement along the 1000-km-long Liquiñe-Ofqui fault from southern Chile (Hernandez-Moreno et al., 2014, 2016):

$$\Theta = 0.5\ D/W$$

Other formulas by Lamb (1987) consider also the occurrence of elongated blocks and their aspect ratio. However, we have no kind of evidence of the shape of the rotating blocks east of the Gaoligong shear zone, so that we assume for simplicity the occurrence of equidimensional blocks.

By considering 165° as maximum CW rotation value (average rotation of sites Yun25 and Yun35, Figures 3 and 8) and 50 and 40 km as total deformation zone width W (although we have no red bed data west of the fault) with respect to the shear zone center (Figure 8a) and the contact with mylonites (Figure 8b), respectively, the formula by Lamb (1987) gives displacement of 290 and 230 km. Such values would be too large if an intracontinental strike-slip fault is considered (Cao, Liu, et al., 2011; Cao, Neubauer, et al., 2011; Otofuji et al., 2010; Tanaka et al., 2008; Tapponnier et al., 1990; Zhong et al., 1991). However, by taking in mind that the Gaoligong shear zone would have bounded rigid blocks—or "microplates"—escaping laterally from the India-Eurasia collision (thus being a sort of transform fault), the 230–290 km offset values given by paleomagnetism become realistic. We remind that an even greater total offset of ~700 km was proposed for the Ailao Shan-Red River shear zone (Chung et al., 1997; Leloup et al., 1995, 2001), although such estimate was considered unrealistically high by other authors (Allen et al., 1984; Replumaz et al., 2001; Schoenbohm et al., 2006; E. C. Wang, Burchfiel, Royden, Chen, et al., 1998).

We note that sites Yun24, Yun42, and Yun29 yield smaller CW (116°, 45°) and 74° CCW rotations (respectively), even if they were sampled adjacent to the fault (Figures 3b and 8). Therefore, it is possible that such sites rotated in fact CW more than 180°.

We conclude that small blocks located adjacent to the fault underwent variable and/or very large CW rotations exceeding largely 180°, but their behavior is not representative of deformation occurring in the 20-km-wide crust slices located at both fault edges. Probably a sort of "rotation channel" exists adjacent to the fault where small blocks rotate freely by large amounts reminding the "ball-bearing model" of Beck (1976).

Average flattening (*F*) values for volcanics and red beds are 12.7° ± 9.4° and 17.4° ± 14.0°, respectively. This confirms that Pliocene-Holocene volcanics have smaller inclinations than those predicted by a GAD field model, likely due to the incomplete averaging of the paleosecular variation of the geomagnetic field. On the other hand, the positive *F* for red beds may be due to the so-called "inclination shallowing," a phenomenon frequently observed in sediments and related to compaction-diagenetic effects on rock fabric and magnetic grains (e.g., Arason & Levi, 1990; Deamer & Kodama, 1990; Tauxe & Kent, 2004). By the way, the positive *F* value would testify that no remagnetization process occurred after sediment diagenesis; thus, it may represent an additional proof for the primary nature of the ChRMs and HT components isolated by us in the red beds.

10. Discussion

Our paleomagnetic transects across the Gaoligong shear zone show that the dextral shear of the fault caused in the Baoshan block CW rotations of the Jurassic-Cretaceous red beds, whose magnitude decreases progressively moving away from the fault (Figure 8). Sites located adjacent to the fault underwent scattered rotations and likely rotated CW by more than 180°. To the west of the fault, Pliocene-Holocene volcanics do not record significant rotations. Rotation of red beds blocks (whose size is likely ≤1 km adjacent to the fault) occurred presumably during the period of main shear zone activity, that is, Oligo-Miocene (Lin et al., 2009; Wang et al., 2006, 2008; Zhang et al., 2012).

Our paleomagnetic data show that the dextral shear along the Gaoligong shear zone ended 5 Ma ago (at least) being later reactivated as sinistral, consistently with the focal mechanism of the 1976 Mw = 7.4 event, that yields for the southern part of the Gaoligong zone a sinistral strike-slip fault kinematics (Figure 1). Moreover, the CW rotation shown today by GPS data in SE Tibet and northern Yunnan (Liang et al., 2013; Figure 1) is certainly not related to the paleomagnetic rotation that ended by 5 Ma.

The paleomagnetism of the Gaoligong shear zone thus suggests that in the Yunnan area, the extrusion of blocks bounded by strike-slip shear zones occurred in Oligo-Miocene times. Such tectonics ceased around 10 Ma (considering the younger Ar/Ar ages provided by Zhang et al., 2012) and was followed by an almost continuous southward drift of Yunnan driven by ductile lower crust squeezed out from Tibet. The present-day southern drift of Yunnan and its collision with Indochina is consistent with both GPS data (Liang et al., 2013; Meade, 2007; Vergnolle et al., 2007) and focal mechanisms of the major earthquakes (Figure 1), yielding ~N-S subhorizontal P axes, thus ~N-S horizontal shortening.

In the past, the predominantly CW rotation pattern of Yunnan (Figure 9) has been related to (1) the lateral extrusion of Tibet describing CW rotation trajectories (Figure 9b; Allmendinger et al., 2007; Copley, 2008; Gan et al., 2007; J. H. Wang et al., 2001; P. Z. Zhang et al., 2004) and (2) large semirigid block rotation driven by strike-slip fault activity following the "broken slate" model (Figure 9a; S. Li, Advokaat, et al., 2017; Tanaka et al., 2008; Yang & Besse, 1993; Yang et al., 2001).

Our data show for the first time that CW rotations in Yunnan are also due to strike-slip fault activity itself and occurred in small (few km of width) blocks inside the 40- to 50-km wide damage zone of the Gaoligong shear zone (total width at both sides of the fault, although we lack red bed data west of the fault). The rotation pattern and block dimensions are consistent with a quasi-continuous crust deformation model (Figure 9c).

However, it is clear that the rotation kinematics of Yunnan is complex and cannot be solely related to the rotation zones bounding the major strike-slip faults. In fact in our working zone, CW rotations of 42°–100° were obtained from 170 to 30 Ma rocks at distances that are generally greater than 20 km from both the Gaoligong and Chongshan shear zones, roughly within the center of the Baoshan and Tengchong blocks (Table 1 and Figure 1, Huang & Opdyke, 1993; Kornfeld, Eckert, Appel, Ratschbacher, Sonntag, et al., 2014; Tong et al., 2016). Thus, such rotations cannot be definitely caused by Gaoligong or Chongshan lateral shear alone. Further east and south of our study area, the recent overview by Li, Advokaat, et al. (2017) similarly suggests a rigid CW rotation for both the Lanping and Simao blocks.

Relying on our and literature data, the rotational behavior of the Baoshan block itself is far from being clear. Tong et al. (2016) reported 70°–80° CW rotations from two localities (NE of Yongde, Figure 1 and Table 1) that are 60–80 km far from the Gaoligong shear zone, thus unquestionably not influenced by fault kinematics. Yet our data suggest that at ~25 km from the contact with fault mylonites, the Baoshan block rotation is virtually annulled (Figure 8b). It is also true, however, that a statistically significant rotation of 20.5° ± 12.2° can be evaluated by considering the four farthest sites from fault contact (Yun03, Yun45, Yun46, and Yun47; Figure 8b). A 20° rigid rotation of the Baoshan block would imply that the maximum rotation value due to fault shear is reduced to 145° (instead of 165°), and this would translate—by using the formula by Lamb (1987)—into a smaller 200–250 km paleomagnetically evaluated Gaoligong fault offset.

We put forward two hypotheses to explain the complexity of the Yunnan rotational pattern:

1. Rotations of the whole Tengchong, Baoshan, and Lanping megablocks coexist with rotations of small blocks (few kilometers in size) inside the fault damage zones (Figure 9). Their relative magnitude and kinematic relation, however, have not been clarified yet;

However, it is difficult to imagine that such elongated rock stripes (400-km long and only 20- to 30-km wide) located between strike-slip faults underwent large rotation, as a big problem of space would arise (Figure 9b). Thus, it is possible that such rotations occurred (at least partly) before that the strike-slip activity of the huge N-S shear zones started in Eocene times.

2. Other unrecognized strike-slip faults exist within the Tengchong and Baoshan blocks, and their activity caused the rotations documented in apparently "undeformed" block centers. Rotating folds and thrust sheets might also contribute to the rotation pattern, as suggested for the Simao block by Kondo et al. (2012), Tong et al. (2013), and Gao et al. (2015).

11. Conclusions

The conclusions of our work can be summarized as follows:

1. The paleomagnetic study of Pliocene-Holocene volcanics and Mesozoic red beds exposed west and east (respectively) of the Gaoligong shear zone show that Ti-poor titanomagnetite and hematite dominate the

respective magnetic mineralogy. Three bits of evidence suggest that the magnetization in the red beds is of primary origin (detrital hematite), and/or acquired during early diagenesis by chemical hematite growth: (1) the data support a positive fold test at the 99% significance level, indicating that magnetization acquisition is pretilting (i.e., pre-Eo-Oligocene) in age; (2) although the majority of the sites yield a normal polarity, three sites show a reverse polarity, and alternating normal and reverse polarity beds were documented in an additional site; (3) a statistically significant positive inclination flattening of the whole red bed data set proves that magnetization acquisition predate diagenesis. Thus, we speculate that—assuming a primary magnetization origin—the majority of our sites were deposited during the long normal Cretaceous superchron. Similar paleomagnetic evidence was previously documented at several other red beds sites from Yunnan (e.g., S. Li, Yang, et al., 2017, and references therein), and the final resolution of this problem would lie in the accurate site age determination, indeed a problematic issue given the continental nature and the coarse grain size of the studied sediments.

2. The clockwise rotations pattern observed in Mesozoic red beds exposed east of the Gaoligong shear zone points to a quasi-continuous crust kinematics model, characterized by rigid blocks of smaller size ($\leq$1 km close to the fault) than the fault deformation zone itself and by rotation values $>$90° close to strike-slip faults. CW rotations close to the fault reach 176° and decrease moving east up to be virtually annulled at ~20 km east from the contact with mylonites exposed along the shear zone (Figure 9c).
3. By using the equation of Lamb (1987), which relates rotations to fault displacement in a quasi-continuous crust deformation model, we find a total Gaoligong fault dextral offset ranging between 230 and 290 km, which is consistent with the 600-km total fault length, if offset is related to megablock extrusion due to India-Asia collision (E. Q. Wang & Burchfiel, 1997; B. Zhang, Zhang, Chang, et al., 2012). Three sites sampled adjacent to the fault yielded scattered rotations (from 74° CCW to 116° CW) that may be interpreted as huge CW rotations exceeding 180°. This suggests that a sort of "rotation channel" exists adjacent to the fault, where small block rotate freely by large magnitude, conforming to the ball-bearing model of Beck (1976).
4. Four sites sampled at greatest distance (15–20 km) from the contact with Gaoligong shear zone mylonites yield a mean CW rotation of 20.5° ± 12.2° (Figure 8b). Although the trend of rotation values versus fault distance is suggestive of a complete rotation cessation at ~25 km from mylonite contact, a 20° rigid CW rotation of the Baoshan block cannot be excluded by our data set. A 20° Baoshan block rotation indeed does not compare with the 70°–80° CW rotations gathered by Tong et al. (2016) from two additional localities from the center of the block itself. A 20° rigid Baoshan block rotation would also reduce to 145° the maximum CW rotation due to Gaoligong fault shear, and this in turn would change to 200–250 km the paleomagnetically evaluated dextral fault offset. However, the discrepancy between our data and those by Tong et al. (2016) strongly suggests that the Baoshan block is broken in additional subblocks undergoing independent rotations.
5. Pliocene-Holocene volcanic sites (and one Pliocene sedimentary site) located west of the fault do not rotate, implying that the Gaoligong dextral shear zone yielding CW rotations has been active during the Oligo-Miocene time span (early Oligocene Gaoligong shear zone activity onset according to Y. J. Wang et al., 2006), but not over the last 5 Ma. This is in good agreement with the focal mechanism of the 1976 Mw = 7.4 earthquake, showing a sinistral shear sense along the southern end of the Gaoligong shear zone and proving that the present-day CW rotation of SE Tibet and northern Yunnan shown GPS data (Liang et al., 2013) has nothing to do with significantly older paleomagnetic rotation. The geomagnetic field PSV is not averaged out in our volcanic paleomagnetic data, thus possibly implying a few degree bias on average null rotation value that is, however, much smaller than the large (up to 176°) rotations observed in Mesozoic red beds.
6. Our work shows for the first time that fault shear may represent a significant tectonics contributing to the CW rotations frequently documented along the Indochina blocks (e.g., S. Li, Advokaat, et al., 2017; Tong et al., 2016). However, CW rotations were also documented far (i.e., $>$20 km) from the strike-slip faults and within the rough center of the blocks themselves, so that it is possible that some blocks—at least the south Indochina, Simao, and Lanping terranes—underwent also semirigid rotations. Yet the tectonics and dynamics of such block rotations (whether a sort of ball-bearing or "domino" model) have not been properly elucidated at presently, and it is unclear why predominantly CW rotations occur. Furthermore, several works (Chen et al., 1995; Sato et al., 2001, 2007; Tanaka et al., 2008) seem to support internal deformation (and variable rotations) in the Simao block, so that no rigid megablock rotation would exist. Kondo

et al. (2012), Tong et al. (2013), and Gao et al. (2015) even report data suggesting a folding-related oroclinal bending within the Simao block itself, which again would be at odds with the rigid "microplate" rotation model proposed by S. Li, Advokaat, et al. (2017). Therefore, we stress that more structural and paleomagnetic work—both in the Yunnan and south Indochina—is needed to properly understand crust kinematics and to untangle the role of faults, small kilometer size block, and mega block rotation and drift on the paleomagnetic rotation pattern.

Acknowledgments
We are grateful to Mu for his kindness and for safely driving us in the whole Yunnan. A. P. acknowledges a PhD grant from University of Catania and B. Z. and C. Y. acknowledge funding by the National Science Foundation of China (NSFC) (41422206). R. M. acknowledges funding by the University of Catania. Publication fees were granted by "Piano per la Ricerca 2016–2018" funding awarded to R. M. Two referees provided detailed reviews of the manuscript. Many thanks to Editors Claudio Faccenna and John Geissman and Associate Editor Augusto Rapalini for carefully evaluating our work. All the data supporting this work (single ChRMs from each sample) have been uploaded in the supporting information section.

References

Akciz, S., Burchfiel, B. C., Crowley, J. L., Yin, J., & Chen, L. (2008). Geometry, kinematics, and regional significance of the Chong Shan shear zone, eastern Himalayan Syntaxis. *Geosphere*, *4*(1), 1–23.

Ali, J. R., Cheung, H. M. C., Aitchison, J. C., & Sun, Y. (2013). Paleomagnetic re-investigations of Early Permian rift basalts from the Baoshan Block, SW China: Constraints on the site-of-origin of the Gondwana-derived eastern Cimmerian terranes. *Geophysical Journal International*, *193*(2), 650–663. https://doi.org/10.1093/gji/ggt012

Allen, C. R., Gillespie, A. R., Han, Y., Sieh, K. E., Zhang, B., & Zhu, C. (1984). Red River and associated faults, Yunnan Province, China. Quaternary geology, slip rates, and seismic hazard. *Geological Society of America Bulletin*, *95*(6), 6686–6700. https://doi.org/10.1130/0016-7606(1984)95%3C686:RRAAFY%3E2.0.CO;2

Allmendinger, R. W., Reilinger, R., & Loveless, J. (2007). Strain and rotation rate from GPS in Tibet, Anatolia and the Altiplano. *Tectonics*, *26*, TC3013. https://doi.org/10.1029/2006TC002030

Arason, P., & Levi, S. (1990). Models of inclination shallowing during sediment compaction. *Journal of Geophysical Research*, *95*, 4481–4499. https://doi.org/10.1029/JB095iB04p04481

Avouac, J.-P., & Tapponnier, P. (1993). Kinematic model of active deformation in central Asia. *Geophysical Research Letters*, *20*, 895–898. https://doi.org/10.1029/93GL00128

Beck, M. E. (1976). Discordant paleomagnetic pole positions as evidence of regional shear in the western Cordillera of North America. *American Journal of Science*, *276*(6), 694–712. https://doi.org/10.2475/ajs.276.6.694

Besse, J., Courtillot, V., Pozzi, J. P., Westphal, M., & Zhou, Y. X. (1984). Paleomagnetic estimates of crustal shortening in the Himalayan thrusts and Zangbo suture. *Nature*, *311*(5987), 621–626. https://doi.org/10.1038/311621a0

Bird, P. (1991). Lateral extrusion of lower crust from under high topography, in the isostatic limit. *Journal of Geophysical Research*, *96*, 10,275–10,286. https://doi.org/10.1029/91JB00370

Bird, P., & Piper, K. (1980). Plane-stress finite element models of tectonic flow in southern California. *Physics of the Earth and Planetary Interiors*, *21*(2-3), 158–175. https://doi.org/10.1016/0031-9201(80)90067-9

Bureau of Geology and Mineral Resources of Xizang Autonomous Region (1993). *Regional geology of Xizang (Tibet) with 1/1,500,000 geological map* (in Chinese with English abstract). Beijing: Geological Publishing House.

Bureau of Geology and Mineral Resources of Yunnan Province (1990). *Regional geology of Yunnan Province* (in Chinese with English Abstract). Beijing: Geological Publishing House.

Cao, S. Y., Liu, J. L., Leiss, B., Neubauer, F., Genser, J., & Zhao, C. Q. (2011). Oligo-Mioceneshearing along the Ailao Shan-Red River shear zone: Constraints from structural analysis and zircon U/Pb geochronology of magmatic rocks in the DiancangShan massif, SE Tibet, China. *Gondwana Research*, *19*(4), 975–993. https://doi.org/10.1016/j.gr.2010.10.006

Cao, S. Y., Neubauer, F., Liu, J. L., Genser, J., & Leiss, B. (2011). Exhumation of the Diancang Shan metamorphic complex along the Ailao Shan-Red River belt, southwestern Yunnan, China: Evidence from $^{40}Ar/^{39}Ar$ thermochronology. *Journal of Asian Earth Sciences*, *42*(3), 525–550. https://doi.org/10.1016/j.jseaes.2011.04.017

Chen, H., Dobson, J., Heller, F., & Hao, J. (1995). Paleomagnetic evidence for clockwise rotation of the Simao region since the Cretaceous: A consequence of India- Asia collision. *Earth and Planetary Science Letters*, *134*, 203–217.

Chung, S.-L., Lee, T.-Y., Lo, C.-H., Wang, P.-L., Chen, C.-Y., TrongYem, N., et al. (1997). Intraplate extension prior to continental extrusion along the Ailao Shan–Red River shear zone. *Geology*, *25*(4), 311–314. https://doi.org/10.1130/0091-7613(1997)025%3C0311:IEPTCE%3E2.3.CO;2

Clark, M. K., Royden, L., Whipple, K., Burchfiel, B., Zhang, X., & Tang, W. (2006). Use of a regional, relict landscape to measure vertical deformation of the eastern Tibetan Plateau. *Journal of Geophysical Research*, *111*, F03002. https://doi.org/10.1029/2005JF000294

Clark, M. K., & Royden, L. H. (2000). Topographic ooze: Building the eastern margin of Tibet by lower crustal flow. *Geology*, *28*(8), 703–706. https://doi.org/10.1130/0091-7613(2000)28%3C703:TOBTEM%3E2.0.CO;2

Cogné, J. P., Besse, J., Chen, Y., & Hankard, F. (2013). A new Late Cretaceous to Present APWP for Asia and its implications for paleomagnetic shallow inclinations in Central Asia and Cenozoic Eurasian plate deformation. *Geophysical Journal International*, *192*(3), 1000–1024. https://doi.org/10.1093/gji/ggs104

Cohen, K. M., Finney, S. C., Gibbard, P. L., & Fan, J.-X. (2013). The ICS international chronostratigraphic chart. *Episodes*, *36*, 199–204.

Copley, A. (2008). Kinematics and dynamics of the southeastern margin of the Tibetan Plateau. *Geophysical Journal International*, *174*(3), 1081–1100. https://doi.org/10.1111/j.1365-246X.2008.03853.x

Cowan, D., Botros, M., & Johnson, H. (1986). Bookshelf tectonics: Rotated crustal blocks within the Sovanco Fracture Zone. *Geophysical Research Letters*, *13*, 995–998. https://doi.org/10.1029/GL013i010p00995

Curray, J. R. (2005). Tectonics and history of the Andaman Sea region. *Journal of Asian Earth Sciences*, *25*(1), 187–232. https://doi.org/10.1016/j.jseaes.2004.09.001

Day, R., Fuller, M., & Schmidt, V. A. (1977). Hysteresis properties of titanomagnetite. Grain-size and compositional dependence. *Physics of the Earth and Planetary Interiors*, *13*(4), 260–267. https://doi.org/10.1016/0031-9201(77)90108-X

Deamer, G. A., & Kodama, K. P. (1990). Compaction-induced inclination shallowing in synthetic and natural clay-rich sediments. *Journal of Geophysical Research*, *95*, 4511–4529. https://doi.org/10.1029/JB095iB04p04511

Demarest, H. (1983). Error analysis for the determination of tectonic rotation from paleomagnetic data. *Journal of Geophysical Research*, *88*, 4321–4328. https://doi.org/10.1029/JB088iB05p04321

Dong, F., Hou, Z., Gao, Y., Zeng, P., & Jiang, C. (2006). Cenozoic granitoid in Tengchong, western Yunnan: Genesis type and implication for tectonics (in Chinese with English abstract). *Acta Petrologica Sinica*, *22*(4), 927–937.

Dunlop, D. J. (2002). Theory and application of the "day plot" (MRS/MS versus Hcr/Hc): Theoretical curves and tests using titanomagnetite data. *Journal of Geophysical Research*, *107*(B3), 2056. https://doi.org/10.1029/2001JB000486

Dziewonski, A. M., Chou, T.-A., & Woodhouse, J. H. (1981). Determination of earthquake source parameters from waveform data for studies of global and regional seismicity. *Journal of Geophysical Research*, *86*, 2825–2852. https://doi.org/10.1029/JB086iB04p02825

Ekström, G., Nettles, M., & Dziewonski, A. M. (2012). The global CMT project 2004-2010: Centroid-moment tensors for 13,017 earthquakes. *Physics of the Earth and Planetary Interiors*, *200-201*(1–9), 1–9. https://doi.org/10.1016/j.pepi.2012.04.002

England, P., & Houseman, G. (1986). Finite strain calculations of continental deformation 2.Comparison with the India-Asia collision zone. *Journal of Geophysical Research*, *91*, 3664–3676. https://doi.org/10.1029/JB091iB03p03664

England, P., Houseman, G., & Sonder, L. (1985). Length scales for continental deformation in convergent, divergent, and strike-slip environments: Analytical and approximate solutions for a thin viscous sheet model. *Journal of Geophysical Research*, *90*, 3551–3557. https://doi.org/10.1029/JB090iB05p03551

England, P., & McKenzie, D. (1982). A thin viscous sheet model for continental deformation. *Geophysical Journal of the Royal Astronomical Society*, *70*(2), 295–321. https://doi.org/10.1111/j.1365-246X.1982.tb04969.x

England, P., & Wells, R. E. (1991). Neogene rotations and quasi-continuous deformation of the Pacific northwest continental margin. *Geology*, *19*(10), 978–981. https://doi.org/10.1130/0091-7613(1991)019%3C0978:NRAQDO%3E2.3.CO;2

Fisher, R. A. (1953). Dispersion on a sphere. *Proceedings of the Royal Society of London, Series A*, *217*(1130), 295–305. https://doi.org/10.1098/rspa.1953.0064

Funahara, S., Nishiwaki, N., Miki, M., Murata, F., Otofuji, Y., & Wang, Y. (1992). Paleomagnetic study of Cretaceous rocks from the Yangtze block, central Yunnan, China: Implications for the India-Asia collision. *Earth and Planetary Science Letters*, *113*(1-2), 77–91. https://doi.org/10.1016/0012-821X(92)90212-E

Funahara, S., Nishiwaki, N., Murata, F., Otofuji, Y., & Wang, Y. Z. (1993). Clockwise rotation of the Red River fault inferred from paleomagnetic study of Cretaceous rocks in the Shan-Thai-Malay Block of western Yunnan, China. *Earth and Planetary Science Letters*, *117*(1-2), 29–42. https://doi.org/10.1016/0012-821X(93)90115-P

Fyhn, M., Boldreel, L. O., & Nielsen, L. H. (2009). Geological development of the central and south Vietnamese margin: Implications for the establishment of the South China Sea, Indochinese escape tectonics and Cenozoic volcanism. *Tectonophysics*, *478*(3–4), 184–214. https://doi.org/10.1016/j.tecto.2009.08.002

Gan, W., Zhang, P., Shen, Z.-K., Niu, Z., Wang, M., Wan, Y., et al. (2007). Present-day crustal motion within the Tibetan plateau inferred from GPS measurements. *Journal of Geophysical Research*, *112*, B08416. https://doi.org/10.1029/2005JB004120

Gao, L., Yang, Z., Tong, Y., Wang, H., & An, C. (2015). New paleomagnetic studies of Cretaceous and Miocene rocks from Jinggu, western Yunnan, China: Evidence for internal deformation of the Lanping–Simao Terrane. *Journal of Geodynamics*, *89*, 39–59. https://doi.org/10.1016/j.jog.2015.06.004

Garfunkel, Z., & Ron, H. (1985). Block rotation and deformation by strike-slip faults: 2. The properties of a type of macroscopic discontinuous deformation. *Journal of Geophysical Research*, *90*, 8589–8602. https://doi.org/10.1029/JB090iB10p08589

Gilley, L. D., Harrison, T. M., Leloup, P. H., Ryerson, F. J., Lovera, O., & Wang, J.-H. (2003). Direct dating of left-lateral deformation along the Red River shear zone, China and Vietnam. *Journal of Geophysical Research*, *108*(B2), 2127. https://doi.org/10.1029/2001JB001726

Hall, R. (2002). Cenozoic geological and plate tectonic evolution of SE Asia and the SW Pacific: Computer-based reconstructions, model and animations. *Journal of Asian Earth Sciences*, *20*(4), 353–431. https://doi.org/10.1016/S1367-9120(01)00069-4

Hall, R., van Hattum, M. W., & Spakman, W. (2008). Impact of India-Asia collision on SE Asia: The record in Borneo. *Tectonophysics*, *451*(1-4), 366–389. https://doi.org/10.1016/j.tecto.2007.11.058

Harrison, R. J., & Feinberg, J. M. (2008). FORCinel: An improved algorithm for calculating first-order reversal curve distributions using locally weighted regression smoothing. *Geochemistry, Geophysics, Geosystems*, *9*, Q05016. https://doi.org/10.1029/2008GC001987

Harrison, T. M., Leloup, P. H., Ryerson, F. J., Tapponnier, P., Lacassin, R., & Chen, W. (1996). Diachronous initiation of transtension along the Ailao Shan–Red River shear zone, Yunnan and Vietnam. In A. Yin & T. M. Harrison (Eds.), *The Tectonic Evolution of Asia* (pp. 208–225). Cambridge: Cambridge University Press.

Hernandez-Moreno, C., Speranza, F., & Di Chiara, A. (2014). Understanding kinematics of intra-arc transcurrent deformation: Paleomagnetic evidence from the Liquiñe-Ofqui fault zone (Chile, 38–41°S). *Tectonics*, *33*, 1964–1988. https://doi.org/10.1002/2014TC003622

Hernandez-Moreno, C., Speranza, F., & Di Chiara, A. (2016). Paleomagnetic rotation pattern of the southern Chile fore-arc sliver (38°S–42°S): A new tool to evaluate plate locking along subduction zones. *Journal of Geophysical Research: Solid Earth*, *121*, 469–490. https://doi.org/10.1002/2015JB012382

Holt, W. E., Ni, J. F., Wallace, T. C., & Haines, A. (1991). The active tectonics of the eastern Himalayan Syntaxis and surrounding regions. *Journal of Geophysical Research*, *96*, 14,595–14,632. https://doi.org/10.1029/91JB01021

Houseman, G., & England, P. (1986). Finite strain calculations of continental deformation 1.Method and general results for convergent ones. *Journal of Geophysical Research*, *91*, 3651–3663. https://doi.org/10.1029/JB091iB03p03651

Houseman, G., & England, P. (1993). Crustal thickening versus lateral expulsion in the Indian-Asian continental collision. *Journal of Geophysical Research*, *98*, 12,233–12,249. https://doi.org/10.1029/93JB00443

Huang, K. N., & Opdyke, N. D. (1991). Paleomagnetic results from the Upper Carboniferous of the Shan-Thai-Malay Block of Western Yunnan, China. *Tectonophysics*, *192*(3-4), 333–344. https://doi.org/10.1016/0040-1951(91)90107-4

Huang, K. N., & Opdyke, N. D. (1993). Paleomagnetic results from Cretaceous and Jurassic rocks of South and Southwest Yunnan: Evidence for large clockwise rotations in the Indochina and Shan-Thai-Malay terranes. *Earth and Planetary Science Letters*, *117*(3-4), 507–524. https://doi.org/10.1016/0012-821X(93)90100-N

Huang, X., Xu, Z., Li, H., & Cai, Z. (2015). Tectonic amalgamation of the Gaoligong shear zone and Lancangjiang shear zone, southeast of Eastern Himalayan Syntaxis. *Journal of Asian Earth Sciences*, *106*, 64–78.https://doi.org/10.1016/j.jseaes.2014.12.018

Ji, J., Zhong, D., & Zhang, L. (2000). The west boundary of Cenozoic extrusion block in Southeast Tibet Plateau. *Chinese Science Bulletin*, *45*(2), 128–134.

Jiang, C. (1998). Distribution characteristics of Tengchong volcano in the Cenozoic era (in Chinese with English abstract). *Journal of Seismology*, *21*(4), 309–319.

Jiang, C., Zhou, R., & Zhao, C. (2003). The relationship between the tectonic geomorphic features and volcano activity in Tengchong Region (in Chinese with English abstract). *Journal of Seismology*, *26*(4), 361–366.

Jiang, Z., Qin, H., Liu, Q., Dekkers, M. J., Tauxe, L., Barron, V., & Torrent, J. (2015). Acquisition of chemical remanent magnetization during experimental ferrihydrite-hematite conversion—Implications for paleomagnetic studies of red beds. *Earth and Planetary Science Letters*, *428*, 1–10.

Kimura, H., Ishikawa, N., & Sato, H. (2011). Estimation of total lateral displacement including strike-slip offset and broader drag deformation on an active fault: Tectonic geomorphic and paleomagnetic evidence on the Tanna fault zone in central Japan. *Tectonophysics*, *501*(1–4), 87–97. https://doi.org/10.1016/j.tecto.2011.01.016

Kimura, H., Itoh, Y., & Tsutsumi, H. (2004). Quaternary strike-slip crustal deformation around an active fault based on paleomagnetic analysis: A case study of the Enako fault in central Japan. *Earth and Planetary Science Letters*, *226*(3-4), 321–334. https://doi.org/10.1016/j.epsl.2004.08.003

Kirschvink, J. L. (1980). The least-squares line and plane and the analysis of paleomagnetic data. *Geophysical Journal of the Royal Astronomical Society*, *62*(3), 699–718. https://doi.org/10.1111/j.1365-246X.1980.tb02601.x

Kondo, K., Mu, C. L., Yamamoto, T., Zaman, H., Miura, D., Yokoyama, M., et al. (2012). Oroclinal origin of the Simao Arc in the Shan-Thai Block inferred from the Cretaceous paleomagnetic data. *Geophysical Journal International*, *190*(1), 201–216. https://doi.org/10.1111/j.1365-246X.2012.05467.x

Kornfeld, D., Eckert, S., Appel, E., Ratschbacher, L., Pfänder, J., Liu, D., & Ding, L. (2014). Clockwise rotation of the Baoshan block due to southeastward tectonic escape of Tibetan crust since the Oligocene. *Geophysical Journal International*, *197*(1), 149–163. https://doi.org/10.1093/gji/ggu09

Kornfeld, D., Eckert, S., Appel, E., Ratschbacher, L., Sonntag, B.-L., Pfänder, J. A., et al. (2014). Cenozoic clockwise rotation of the Tengchong block, southeastern Tibetan Plateau: A paleomagnetic and geochronologic study. *Tectonophysics*, *628*, 105–122.

Kornfeld, D., Sonntag, B.-L., Gast, S., Matthes, J., Ratschbacher, L., Pfänder, J. A., et al. (2014). Apparent paleomagnetic rotations reveal Pliocene–Holocene internal deformation of the Tengchong Block, southeastern Tibetan Plateau. *Journal of Asian Earth Sciences*, *96*, 1–16.

Laccassin, R., Replumaz, A., & Leloup, P. H. (1998). Hairpin river loops and slip-sense inversion on southeast Asian strike–slip faults. *Geology*, *26*(8), 703–706. https://doi.org/10.1130/0091-7613(1998)026%3C0703:HRLASS%3E2.3.CO;2

Lamb, S. H. (1987). A model for tectonic rotations about a vertical axis. *Earth and Planetary Science Letters*, *84*(1), 75–86. https://doi.org/10.1016/0012-821X(87)90178-6

Leloup, P. H., Arnaud, N., Lacassin, R., Kienast, J. R., Harrison, T. M., PhanTrong, T., et al. (2001). New constraints on the structure, thermochronology and timing of the Ailao Shan-Red River shear zone, SE Asia. *Journal of Geophysical Research*, *106*, 6657–6671.

Leloup, P. H., & Kienast, J.-R. (1993). High temperature metamorphism in a major strike slip shear zone: The Ailao Shan Red River, People's Republic of China. *Earth and Planetary Science Letters*, *118*, 213–234.

Leloup, P. H., Lacassin, R., Tapponnier, P., Zhong, D., Liu, X., Zhang, L., et al. (1995). The Ailao Shan-Red River shear zone (Yunnan, China), Tertiary transform boundary of Indochina. *Tectonophysics*, *251*, 3–84.

Li, D., Li, Q., & Chen, W. (2000). Volcanic activities in the Tengchong volcano area since Pliocene (in Chinese with English abstract). *Acta Petrologica Sinica*, *16*, 362–370.

Li, D. M., Li, Q., & Chen, W. J. (1999). Excess argon in plagioclase phenocryst of Tengchong volcanics and the related volcano erupting stages (in Chinese with English abstract). *Geology Reviews*, *45*, 892–894.

Li, H., Xu, Z., Cai, Z., Tang, Z., & Yang, M. (2011). Indosinian epoch magmatic event and geological significance in the Tengchong block, western Yunnan Province (in Chinese with English abstract). *Acta Petrologica Sinica*, *27*(7), 2165–2172.

Li, P., Rui, G., Cui, J., & Ye, G. (2004). Paleomagnetic analysis of eastern Tibet: Implications for the collision and amalgamation history of the Three River Region, SW China. *Journal of Asian Earth Sciences*, *24*(3), 291–310. https://doi.org/10.1016/j.jseaes.2003.12.003

Li, S., Advokaat, E. L., Van Hinsbergen, D. J. J., Koymans, M., Deng, C., & Zhu, R. (2017). Paleomagnetic constraints on the Mesozoic-Cenozoic paleolatitudinal and rotational history of Indochina and South China: Review and updated kinematic reconstruction. *Earth Science Reviews*, *171*, 58–77. https://doi.org/10.1016/j.earscirev.2017.05.007

Li, S., Yang, Z., Deng, C., He, H., Qin, H., Sun, L., et al. (2017). Clockwise rotations recorded in redbeds from the Jinggu Basin of northwestern Indochina. *Geological Society of America Bulletin*. https://doi.org/10.1130/B31637.1

Liang, S., Gan, W., Shen, C., Xiao, G., Liu, J., Chen, W., et al. (2013). Three-dimensional velocity field of present-day crustal motion of the Tibetan Plateau derived from GPS measurements. *Journal of Geophysical Research: Solid Earth*, *118*, 5722–5732. https://doi.org/10.1002/2013JB010503

Lin, T. H., Lo, C. H., Chung, S. L., Hsu, F. J., Yeh, M. W., Lee, T. Y., et al. (2009). $^{40}Ar/^{39}Ar$ dating of the Jiali and Gaoligong shear zones: Implications for crustal deformation around the Eastern Himalayan Syntaxis. *Journal of Asian Earth Sciences*, *34*, 674–685.

Liu-Zeng, J., Tapponnier, P., Gaudemer, Y., & Ding, L. (2008). Quantifying landscape differences across the Tibetan plateau: Implications for topographic relief evolution. *Journal of Geophysical Research*, *113*, F04018. https://doi.org/10.1029/2007JF000897

Mandl, G. (1987). Tectonic deformation by rotating parallel faults: The "bookshelf" mechanism. *Tectonophysics*, *141*(4), 277–316. https://doi.org/10.1016/0040-1951(87)90205-8

McFadden, P. L. (1990). A new fold test for paleomagnetic studies. *Geophysical Journal International*, *103*(1), 163–169. https://doi.org/10.1111/j.1365-246X.1990.tb01761.x

McFadden, P. L., & McElhinny, M. W. (1990). Classification of the reversal test in paleomagnetism. *Geophysical Journal International*, *130*, 725–729.

McKenzie, D., & Jackson, J. (1983). The relationship between strain rates, crustal thickening, palaeomagnetism, finite strain and fault movements within a deforming zone. *Earth and Planetary Science Letters*, *65*(1), 182–202. https://doi.org/10.1016/0012-821X(83)90198-X

McKenzie, D., & Jackson, J. (1986). A block model of distributed deformation by faulting. *Journal of the Geological Society of London*, *143*(2), 349–353. https://doi.org/10.1144/gsjgs.143.2.0349

Meade, B. J. (2007). Present-day kinematics at the India-Asia collision zone. *Geology*, *35*(1), 81–84. https://doi.org/10.1130/G22924A.1

Metacalfe, I. (2013). Gondwana dispersion and Asian accretion: Tectonic and palaeogeographic evolution of eastern Tethys. *Journal of Asian Earth Sciences*, *66*, 1–33.

Metcalfe, I. (2002). Permian tectonic framework and palaeogeography of SE Asia. *Journal of Asian Earth Sciences*, *20*(6), 551–566. https://doi.org/10.1016/S1367-9120(02)00022-6

Metcalfe, I. (2006). Paleozoic and Mesozoic tectonic evolution and palaeogeography of East Asian crustal fragments: The Korean peninsula in context. *Gondwana Research*, *9*(1-2), 24–46. https://doi.org/10.1016/j.gr.2005.04.002

Metcalfe, I. (2011). Palaeozoic–Mesozoic history of SE Asia. In R. Hall, M. Cottam, & M. Wilson (Eds.), *The SE Asian gateway: History and tectonics of Australia–Asia collision. Geological Society of London, Special Publications*, 355, 7–35.

Mitchell, A. H. G. (1992). Late Permian–Mesozoic events and the Mergui group nappe in Myanmar and Thailand. *Journal of Southeast Asian Earth Sciences*, *7*(2-3), 165–178. https://doi.org/10.1016/0743-9547(92)90051-C

Mitchell, A. H. G. (1993). Cretaceous-Cenozoic tectonic events in western Myanmar (Burma)-Assam region. *Journal of the Geological Society of London*, *150*(6), 1089–1102. https://doi.org/10.1144/gsjgs.150.6.1089

Molnar, P., & Dayem, K. E. (2010). Major intracontinental strike-slip faults and contrasts in lithospheric strength. *Geoshpere*, *6*(4), 444–467.

Molnar, P., Parco-Casas, F., & Stock, J. (1988). The Cenozoic and Late Cretaceous evolution of the Indian Ocean Basin: Uncertainties in the reconstructed positions of the Indian, African and Antarctic plates. *Basin Research*, *1*(1), 23–40. https://doi.org/10.1111/j.1365-2117.1988.tb00003.x

Molnar, P., & Tapponnier, P. (1975). Cenozoic tectonics of Asia: Effects of a continental collision. *Science*, *189*(4201), 419–426. https://doi.org/10.1126/science.189.4201.419

Morley, C. K. (2007). Variation in Late Cenozoic-recent strike-slip and oblique-extensional geometries, within Indochina: The influence of pre-existing fabrics. *Journal of Structural Geology*, *29*(1), 36–58. https://doi.org/10.1016/j.jsg.2006.07.003

Mu, Z., Tong, W., & Garniss, H. C. (1987). Times of volcanic activity and origin of magma in Tengchong geothermal area, West Yunnan province (in Chinese with English abstract). *Acta Geophysica Sinica*, *30*(3), 261–270.

Najman, Y., Appel, E., Boudagher-Fadel, M., Brown, P., Carter, A., Garzanti, E., et al. (2010). Timing of India–Asia collision: Geological, biostratigraphic, and paleomagnetic constraints. *Journal of Geophysical Research*, *115*, B12416. https://doi.org/10.1029/2010JB007673

Nelson, M., & Jones, C. (1987). Paleomagnetism and crustal rotations along a shear zone, Las Vegas Range, southern Nevada. *Tectonics*, *6*, 13–33. https://doi.org/10.1029/TC006i001p00013

Nur, A., Ron, H., & Scotti, O. (1986). Fault mechanics and the kinematics of block rotations. *Geology*, *14*, 746–749. https://doi.org/10.1130/0091-7613(1986)14%3C746

Ogg, J. G. (2012). Geomagnetic Polarity Time Scale. In *The Geologic Time Scale* (chap. 5, pp. 85–113). Boston: Elsevier. https://doi.org/10.1016/B978-0-444-59425-9.00005-6

Otofuji, Y., Yokoyama, M., Kitada, K., & Zaman, H. (2010). Paleomagnetic versus GPS determined tectonic rotation around eastern Himalayan Syntaxis in East Asia. *Journal of Asian Earth Sciences*, *37*, 438–451.

Patriat, P., & Achache, J. (1984). India-Eurasia collision chronology has implications for crustal shortening and driving mechanism of plates. *Nature*, *311*(5987), 615–621. https://doi.org/10.1038/311615a0

Peltzer, G., & Tapponnier, P. (1988). Formation and evolution of strike-slip faults, rifts, and basins during the India-Asia collision: An experimental approach. *Journal of Geophysical Research*, *93*, 15,085–15,117.

Petrovský, E., & Kapička, A. (2006). On determination of the Curie point from thermomagnetic curves. *Journal of Geophysical Research*, *111*, B12S27. https://doi.org/10.1029/2006JB004507

Pike, C. R., Roberts, A. P., & Verosub, K. L. (1999). Characterizing interactions in fine magnetic particle systems using first order reversal curves. *Journal of Applied Physics*, *85*(9), 6660–6667. https://doi.org/10.1063/1.370176

Pike, C. R., Roberts, A. P., & Verosub, K. L. (2001). First-order reversal curve diagrams and thermal relaxation effects in magnetic particles. *Geophysical Journal International*, *145*(3), 721–730.

Piper, J., Tatar, O., & Gürsoy, H. (1997). Deformational behavior of continental lithosphere deduced from block rotations across the North Anatolian Fault Zone in Turkey. *Earth and Planetary Science Letters*, *150*(3-4), 191–203. https://doi.org/10.1016/S0012-821X(97)00103-9

Randall, K., Lamb, S., & Mac Niocaill, C. (2011). Large tectonic rotations in a wide zone of Neogene distributed dextral shear, northeastern South Island, New Zealand. *Tectonophysics*, *509*(3–4), 165–180. https://doi.org/10.1016/j.tecto.2011.05.006

Ratschbacher, L., Frisch, W., Chen, C., & Pan, G. (1996). Cenozoic deformation, rotation, and stress patterns in eastern Tibet and western Sichuan, China. In A. Yin & T. M. Harrison (Eds.), *The Tectonic Evolution of Asia* (pp. 227–249). Cambridge: Cambridge University Press.

Replumaz, A., Lacassin, R., Tapponnier, P., & Leloup, P. H. (2001). Large river offsets and Plio-quaternary dextral slip rate on the Red River fault (Yunnan, China). *Journal of Geophysical Research*, *106*, 819–836. https://doi.org/10.1029/2000JB900135

Replumaz, A., & Tapponnier, P. (2003). Reconstruction of the deformed collision zone between India and Asia by backward motion of lithospheric blocks. *Journal of Geophysical Research*, *108*(B6), 2285. https://doi.org/10.1029/2001JB000661

Roberts, A. P., Cui, Y., & Verosub, K. L. (1995). Wasp-waisted hysteresis loops: Mineral magnetic characteristics and discrimination of components in mixed magnetic systems. *Journal of Geophysical Research*, *100*, 17,909–17,924. https://doi.org/10.1029/95JB00672

Roberts, A. P., Pike, C. R., & Verosub, K. L. (2000). First order reversal curve diagrams: a new tool for characterizing the magnetic properties of natural samples. *Journal of Geophysical Research*, *105*, 28,461–28,475. https://doi.org/10.1029/2000JB900326

Roger, F., Calassou, S., Lancelot, J., Malavieille, J., Mattauer, M., Xu, Z., et al. (1995). Miocene emplacement and deformation of the Konga Shan granite (Xianshui He fault zone, West Sichuan, China): Geodynamic implications. *Earth and Planetary Science Letters*, *130*, 201–216.

Ron, H., Freund, R., Garfunkel, Z., & Nur, A. (1984). Block rotation by strike-slip faulting: Structural and paleomagnetic evidence. *Journal of Geophysical Research*, *89*, 6256–6270. https://doi.org/10.1029/JB089iB07p06256

Royden, L. H., Burchfiel, B. C., King, R., Wang, E., Chen, Z., Shen, F., & Liu, Y. (1997). Surface deformation and lower crustal flow in eastern Tibet. *Science*, *276*(5313), 788–790. https://doi.org/10.1126/science.276.5313.788

Royden, L. H., Burchfiel, B. C., & Van der Hilst, R. D. (2008). The geological evolution of the Tibetan Plateau. *Science*, *321*(5892), 1054–1058. https://doi.org/10.1126/science.1155371

Sato, K., Liu, Y. Y., Wang, Y. B., Yokoyama, M., Yoshioka, S., Yang, Z. Y., & Otofuji, Y. (2007). Paleomagnetic study of Cretaceous rocks from Pu'er, western Yunnan, China: Evidence of internal deformation of the Indochina Block. *Earth and Planetary Science Letters*, *258*(1-2), 1–15. https://doi.org/10.1016/j.epsl.2007.02.043

Sato, K., Liu, Y. Y., Zhu, Z. C., Yang, Z. Y., & Otofuji, Y. (1999). Paleomagnetic study of middle Cretaceous rocks from Yunlong, western Yunnan, China: Evidence of south-ward displacement of Indochina. *Earth and Planetary Science Letters*, *165*, 1–15.

Sato, K., Liu, Y. Y., Zhu, Z. C., Yang, Z. Y., & Otofuji, Y. (2001). Tertiary paleomagnetic data from northwestern Yunnan, China: Further evidence for large clockwise rotation of the Indochina Block and its tectonic implications. *Earth and Planetary Science Letters*, *185*(1-2), 185–198. https://doi.org/10.1016/S0012-821X(00)00377-0

Schärer, U., Zhang, L. S., & Tapponnier, P. (1994). Duration of strike-slip movements in large shear zones: The Red River belt, China. *Earth and Planetary Science Letters*, *126*, 379–397.

Schoenbohm, L. M., Burchfiel, B. C., Chen, L., & Yin, J. (2006). Miocene to present activity along the Red River fault, China, in the context of continental extrusion, upper crustal rotation, and lower-crustal flow. *Geological Society of America Bulletin*, *118*(5-6), 672–688. https://doi.org/10.1130/B25816.1

Searle, M. P. (2006). Role of the Red River shear zone, Yunnan and Vietnam, in the continental extrusion of SE Asia. *Journal of the Geological Society, London*, *163*(6), 1025–1036. https://doi.org/10.1144/0016-76492005-144. Printed in Great Britain

Searle, M. P., Noble, S. R., Cottle, J. M., Waters, D. J., Mitchell, A. H. G., Hlaing, T., & Horstwood, M. S. A. (2007). Tectonic evolution of the Mogok metamorphic belt, Burma (Myanmar) constrained by U–Th–Pb dating of metamorphic and magmatic rocks. *Tectonics*, *26*, TC3014. https://doi.org/10.1029/2006TC002083

Socquet, A., & Pubellier, M. (2005). Cenozoic deformation in western Yunnan (China–Myanmar border). *Journal of Asian Earth Sciences*, *24*(4), 495–515. https://doi.org/10.1016/j.jseaes.2004.03.006

Sonder, L., & England, P. (1986). Vertical averages of rheology of the continental lithosphere: Relation to thin sheet parameters. *Earth and Planetary Science Letters*, *77*(1), 81–90. https://doi.org/10.1016/0012-821X(86)90134-2

Sonder, L. J., England, P. C., & Houseman, G. A. (1986). Continuum calculation of continental deformation in transcurrent environments. *Journal of Geophysical Research*, *91*, 4797–4810. https://doi.org/10.1029/JB091iB05p04797

Sonder, L. J., Jones, C. H., Salyards, S. L., & Murphy, K. M. (1994). Vertical axis rotations in the Las Vegas Valley Shear Zone, southern Nevada: Paleomagnetic constraints on kinematics and dynamics of block rotations. *Tectonics*, *13*, 769–788. https://doi.org/10.1029/94TC00352

Tanaka, K., Mu, C. L., Sato, K., Takemoto, K., Miura, D., Liu, Y. Y., et al. (2008). Tectonic deformation around the eastern Himalayan Syntaxis: Constraints from the Cretaceous palaeomagnetic data of the Shan-Thai Block. *Geophysical Journal International*, *175*, 713–728.

Tapponnier, P., Lacassin, R., Leloup, P. H., Schärer, U., Zhong, D. L., Liu, X. H., et al. (1990). The Ailao Shan–Red River metamorphic belt: Tertiary left lateral shear between Sundaland and South China. *Nature*, *343*(6257), 431–437. https://doi.org/10.1038/343431a0

Tapponnier, P., & Molnar, P. (1976). Slip line field theory and large-scale continental tectonics. *Nature*, *264*(5584), 319–324. https://doi.org/10.1038/264319a0

Tapponnier, P., & Molnar, P. (1977). Active faulting and tectonics in China. *Journal of Geophysical Research*, *82*, 2905–2930. https://doi.org/10.1029/JB082i020p02905

Tapponnier, P., Peltzer, G., & Armijo, P. (1986). On the mechanics of the collision between India and Asia. In M. P. Coward & A. C. Ries (Eds.), *Collision Tectonics. Geological Society of London, Special Publication*, 19, 115–157.

Tapponnier, P., Peltzer, G., Armijo, R., Le Dain, A.-Y., & Cobbold, P. (1982). Propagating extrusion tectonics in Asia: New insights from simple experiments with plasticine. *Geology*, *10*(12), 611–616. https://doi.org/10.1130/0091-7613(1982)10%3C611:PETIAN%3E2.0.CO;2

Tauxe, L. (2005). Inclination flattening and the geocentric axial dipole hypothesis. *Earth and Planetary Science Letters*, *233*(3-4), 247–261. https://doi.org/10.1016/j.epsl.2005.01.027

Tauxe, L., & Kent, D. V. (2004). A simplified statistical model for the geomagnetic field and the detection of shallow bias in paleomagnetic inclinations: Was the ancient magnetic field dipolar? In J. E. T. Channell, et al. (Eds.), *Timescales of the paleomagnetic field, Geophysical Monographic Series* (Vol. 145, pp. 101–115). Washington, DC: American Geophysical Union.

Tong, Y., Yang, Z., Jing, X., Zhao, Y., Li, C., Huang, D., & Zhang, X. (2016). New insights into the Cenozoic lateral extrusion of crustal blocks on the southeastern edge of Tibetan Plateau: Evidence from paleomagnetic results from Paleogene sedimentary strata of the Baoshan Terrane. *Tectonics*, *35*, 2494–2514. https://doi.org/10.1002/2016TC004221

Tong, Y. B., Yang, Z. Y., Zheng, L. D., Xu, Y. L., Wang, H., Gao, L., & Hu, X. Z. (2013). Internal crustal deformation in the northern part of Shan-Thai Block: New evidence from paleomagnetic results of Cretaceous and Paleogene redbeds. *Tectonophysics*, *608*, 1138–1158. https://doi.org/10.1016/j.tecto.2013.06.031

Torsvik, T. H., Van der Voo, R., Preeden, U., Mac Niocaill, C., Steinberger, B., Doubrovine, P. V., et al. (2012). Phanerozoic polar wander, paleogeography and dynamics. *Earth-Science Reviews*, *114*(3-4), 325–368. https://doi.org/10.1016/j.earscirev.2012.06.007

Tucker, R. T., Zou, H., Fan, Q., & Schmitt, A. K. (2013). Ion microprobe dating of zircons from active Dayingshan volcano, Tengchong, SE Tibetan Plateau: Time scales and nature of magma chamber storage. *Lithos*, *172–173*, 214–221.

Vergnolle, M., Calais, E., & Dong, L. (2007). Dynamics of continental deformation in Asia. *Journal of Geophysical Research*, *112*, B11403. https://doi.org/10.1029/2006JB004807

Vilotte, J. P., Madariaga, R., Daignieres, M., & Zienkiewicz, O. (1986). Numerical study of continental collision: Influence of buoyancy forces and an initial inclusion. *Geophysical Journal International*, *84*(2), 279–310. https://doi.org/10.1111/j.1365-246X.1986.tb04357.x

Wang, E., & Burchfiel, B. C. (1997). Interpretation of Cenozoic tectonics in the right- lateral accommodation zone between the Ailao Shan shear zone and the eastern Himalayan Syntaxis. *International Geology Review*, *39*(3), 191–219. https://doi.org/10.1080/00206819709465267

Wang, E., & Burchfiel, B. C. (2000). Late Cenozoic to Holocene deformation in south-western Sichuan and adjacent Yunnan, China, and its role in formation of the southeastern part of the Tibetan Plateau. *Geological Society of America Bulletin*, *112*, 413–423.

Wang, E. C., Burchfiel, B. C., Royden, L. H., Chen, L. Z., Li, W. X., & Chen, Z. L. (1998). Late Cenozoic Xianshuihe–Xiaojiang, Red River, and Dali Fault Systems of Southwestern Sichuan and Central Yunnan, China. *Geological Society of America Special Papers*, *327*, 1–108.

Wang, E. C., Burchfiel, B. C., & Royden, R. H. (1998). Late Cenozoic compressional deformations and their origin along the Xiaojiang strike-slip fault system in Central Yunnan, China. *Scientia Geologica Sinica*, *30*(3), 209–219.

Wang, F., Chen, W. J., Pen, Z. C., Zhang, Z. L., & Hu, Y. T. (1999). Chronology of young volcanic rocks of Changbaishan Tianchi and Tengchong, China, by using the Uranium-series TIMS method (in Chinese with English abstract). *Geology Reviews*, *45*, 914–925.

Wang, G., Wan, J., Wang, E., Zheng, D., & Li, F. (2008). Late Cenozoic to recent transtensional deformation across the southern part of the Gaoligong shear zone between the Indian plate and SE margin of the Tibetan plateau and its tectonic origin. *Tectonophysics*, *460*(1-4), 1–20. https://doi.org/10.1016/j.tecto.2008.04.007

Wang, J. H., Yin, A., Harrison, T. M., Grove, M., Zhang, Y.-Q., & Xie, G.-H. (2001). A tectonic model for Cenozoic igneous activities in the eastern Indo–Asian collision zone. *Earth and Planetary Science Letters*, *188*, 123–133.

Wang, P.-L., Lo, C.-H., Lee, T.-Y., Chung, S.-L., Lan, C.-Y., & Yem, N. T. (1998). Thermochronological evidence for the movement of the Ailao Shan–Red River shear zone: A perspective from Vietnam. *Geology*, *26*, 897–890.

Wang, Y., Zhang, X., Jiang, C., Wei, H., & Wan, J. (2007). Tectonic controls on the late Miocene–Holocene volcanic eruptions of the Tengchong volcanic field along the southeastern margin of the Tibetan plateau. *Journal of Asian Earth Sciences*, *30*(2), 375–389.

Wang, Y. J., Fan, W. M., Zhang, Y. H., Peng, T. P., Chen, X. Y., & Xu, Y. G. (2006). Kinematics and $^{40}Ar/^{39}Ar$ geochronology of the Gaoligong and Chongshan shear systems, western Yunnan, China: Implications for early Oligocene tectonic extrusion of SE Asia. *Tectonophysics*, *418*, 235–254.

Xu, Y., Yang, Q., Lan, J., Luo, Z., Huang, X., Shi, Y., & Xie, L. (2012). Temporal-spatial distribution and tectonic implications of the batholiths in the Gaoligong-Tengliang-Yingjiang area, western Yunnan: Constraints from zircon U-Pb ages and Hf isotopes. *Journal of Asian Earth Sciences*, *53*, 151–175. https://doi.org/10.1016/j.jseaes.2011.06.018

Xu, Z. Q., Wang, Q., Cai, Z. H., Dong, H. W., Li, H. Q., Chen, X. J., et al. (2015). Kinematics of the Tengchong Terrane in SE Tibet from the late Eocene to early Miocene: Insights from coeval mid-crustal detachments and strike-slip shear zones. *Tectonophysics*, *665*, 127–148. https://doi.org/10.1016/j.tecto.2015.09.033

Yang, Z. Y., & Besse, J. (1993). Paleomagnetic study of Permian and Mesozoic sedimentary rocks from northern Thailand supports the extrusion model for Indochina. *Earth and Planetary Science Letters*, *117*(3-4), 525–552. https://doi.org/10.1016/0012-821X(93)90101-E

Yang, Z. Y., & Otofuji, Y. (2001). Paleomagnetic study of the Early Tertiary on both sides of the Red River fault and its geological implications. *Acta Geologica Sinica*, *75*(1), 35–44.

Yang, Z. Y., Yin, J. Y., Sun, Z. M., Otofuji, Y., & Sato, K. (2001). Discrepant Cretaceous paleomagnetic poles between Eastern China and Indochina: A consequence of the extrusion of Indochina. *Tectonophysics*, *334*(2), 101–113. https://doi.org/10.1016/S0040-1951(01)00061-0

Yin, A. (2010). Cenozoic tectonic evolution of Asia: A preliminary synthesis. *Tectonophysics*, *488*(1-4), 293–325. https://doi.org/10.1016/j.tecto.2009.06.002

Yin, A., & Harrison, T. M. (2000). Geologic evolution of the Himalaya–Tibetan orogen. *Annual Review of Earth and Planetary Sciences*, *28*(1), 211–280. https://doi.org/10.1146/annurev.earth.28.1.211

Yin, A., & Taylor, M. H. (2011). Mechanics of V-shaped conjugate strike-slip faults and the corresponding continuum mode of continental deformation. *Geological Society of America Bulletin*, *123*(9–10), 1798–1821. https://doi.org/10.1130/B30159.1

Zhang, B., Zhang, J., Chang, Z., Wang, X., Cai, F., & Lai, Q. (2012). The Biluoxueshan transpressive deformation zone monitored by synkinematic plutons, around the Eastern Himalayan Syntaxis. *Tectonophysics*, *574*, 158–180.

Zhang, B., Zhang, J. J., & Zhong, D. L. (2010). Structure, kinematics and ages of transpression during strain partitioning in the Chongshan shear zone, western Yunnan, China. *Journal of Structural Geology*, *32*(4), 445–463. https://doi.org/10.1016/j.jsg.2010.02.001

Zhang, B., Zhang, J. J., Zhong, D. L., Wang, X. X., Qu, J. F., & Guo, L. (2011). Structural feature and its significance of the northernmost segment of the Tertiary Biluoxueshan-Chongshan shear zone, east of the eastern Himalayan Syntaxis. *Science China Earth Sciences*, *54*(7), 959–974. https://doi.org/10.1007/s11430-011-4197-y

Zhang, B., Zhang, J. J., Zhong, D. L., Yang, L. K., Yue, Y. H., & Yan, S. Y. (2012). Polystage deformation of the Gaoligong metamorphic zone: Structures, $^{40}Ar/^{39}Ar$ mica ages, and tectonic implications. *Journal of Structural Geology*, *37*, 1–18.

Zhang, J. J., Zhong, D. L., Sang, H. Q., & Zhou, Y. (2006). Structural and geochronological evidence for multiple episodes of Tertiary deformation along the AilaoShan–Red River shear zone, Southeastern Asia, since the Paleocene. *Acta Geologica Sinica*, *80*, 79–96.

Zhang, L., & Zhong, D. (1996). The Red River strike-slip shear zone and Cenozoic tectonics of East Asia continent (in Chinese with English abstract). *Scientia Geologica Sinica*, *31*(4), 327–341.

Zhang, P. Z., Shen, Z., Wang, M., Gan, W. J., Burgmann, R., & Molnar, P. (2004). Continuous deformation of the Tibetan Plateau from global positioning system data. *Geology*, *32*(9), 809–812. https://doi.org/10.1130/G20554.1

Zhang, R., Cong, B., Maruyama, S., & Liou, J. G. (1993). Metamorphism and tectonic evolution of the Lancang paired metamorphic belts, southwestern China. *Journal of Metamorphic Geology*, *11*(4), 605–619. https://doi.org/10.1111/j.1525-1314.1993.tb00175.x

Zhang, S. C., Diao, G. L., Wang, S. J., & Long, X. F. (1994). Rupture characteristics of the 1976 Longling earthquake sequence (in Chinese with English abstract). *Earthquake Research in China*, *10*(2), 152–159.

Zhao, C. H., & Chen, T. F. (1992). A discussion on magma-tectonic type of Cenozoic volcanism from Tengchong area (Yunnan Province)—A new type of post-collision arc-volcanism (in Chinese with English abstract). *Geoscience*, *6*, 119–129.

Zhao, J., Huang, B. C., Yang, Y. G., & Zhang, D. H. (2015). Late Triassic paleomagnetic result from the Baoshan Terrane, West Yunnan of China: Implication for orientation of the East Paleotethys suture zone and timing of the Sibumasa-Indochina collision. *Journal of Asian Earth Sciences*, *111*, 350–364. https://doi.org/10.1016/j.jseaes.2015.06.033

Zhong, D. L. (1998). *The Paleo-Tethyan orogenic belts, western Yunnan and Sichun Provinces* (pp. 1–231). Beijing: *Science Press*. (in Chinese)

Zhong, D. L. (2000). *Paleotethyan orogenic belts in Yunnan and Western Sichuan* (pp. 230–240). Beijing: Science Press.

Zhong, D. L., & Tapponnier, P. (1990). Large-scale strike slip fault: The major structure of intracontinental deformation after collision. *Chinese Science Bulletin*, *35*, 304–309.

Zhong, D. L., Wang, Y., & Ding, L. (1991). The tertiary Gaoligong intracontinental strike-slip fault and its associated extensional structure in western Yunnan, China (in Chinese with English abstract). In X. Zhang (Ed.), *Annual Report 1989–1990 Lab*, *Lithos. Tecton. Evolution. Inst. Geol*. (pp. 18–22). Beijing: Academia Sinica.

Zhu, B. Q., Mao, C. X., Lugmair, G. W., & Macdougall, J. D. (1983). Isotopic and geochemical evidence for the origin of Plio-Pleistocene volcanic rocks near the Indo-Eurasian collisional margin at Tengchong, China. *Earth and Planetary Science Letters*, *65*(2), 263–275.

Zijderveld, J. D. (1967). A. C. Demagnetization of rocks: Analysis of results. In D. W. Collinson, K. M. Creer, & S. K. Runcorn (Eds.), *Methods in paleomagnetism* (pp. 254–286). New York: Elsevier.

Zou, H., Fan, Q., Schmitt, A. K., & Sui, J. (2010). U–Th dating of zircons from Holocene Potassic andesites (Maanshan volcano, Tengchong, SE Tibetan Plateau) by depth profiling: Time scales and nature of magma storage. *Lithos*, *118*(1–2), 202–210.

Zou, H., Shen, C.-C., Fan, Q., & Lin, K. (2014). U-series disequilibrium in young Tengchong volcanics: Recycling of mature clay sediments or mudstones into the SE Tibetan mantle. *Lithos*, *192–195*, 132–141.